Inorganic Chemistry

Article

pubs.acs.org/IC

Synthesis and Characterization of $(smif)_2M^n$ (n = 0, M = V, Cr, Mn, Fe, Co, Ni, Ru; n = +1, M = Cr, Mn, Co, Rh, Ir; smif =1,3-di-(2-pyridyl)-2-azaallyl)

Brenda A. Frazier,[†] Erika R. Bartholomew,[†] Peter T. Wolczanski,*[,†] Serena DeBeer,[†,⊥] Mitk'El Santiago-Berrios,[†] Hector D. Abruña,[†] Emil B. Lobkovsky,[†] Suzanne C. Bart,[‡] Susanne Mossin,[‡] Karsten Meyer,[‡] and Thomas R. Cundari[§]

[†]Department of Chemistry & Chemical Biology, Baker Laboratory, Cornell University, Ithaca, New York 14853, United States

[‡]Department of Chemistry & Pharmacy, University of Erlangen-Nuremberg, Egerlandstrasse 1, D-91058 Erlangen, Germany

[§]Department of Chemistry, Center for Advanced Scientific Computing and Modeling (CASCaM), University of North Texas, Box 305070, Denton, Texas 76203-5070, United States

Supporting Information

ABSTRACT: A series of Werner complexes featuring the tridentate ligand smif, that is, 1,3-di-(2-pyridyl)-2-azaallyl, have been prepared. Syntheses of $(smif)_2M$ (**1**-M; M = Cr, Fe) were accomplished via treatment of $M(NSiMe_3)_2(THF)_n$ (M = Cr, n = 2; Fe, n = 1) with 2 equiv of (smif)H (1,3-di-(2-pyridyl)-2-azapropene); *ortho*-methylated $(^oMesmif)_2Fe$ (**2**-Fe) and $(^oMe_2smif)_2Fe$ (**3**-Fe) were similarly prepared. Metatheses of MX_2 variants with 2 equiv of Li(smif) or Na(smif) generated **1**-M (M = Cr, Mn, Fe, Co, Ni, Zn, Ru). Metathesis of $VCl_3(THF)_3$ with 2 Li(smif) with a reducing equiv of Na/Hg present afforded **1**-V, while 2 Na(smif) and $IrCl_3(THF)_3$ in the presence of $NaBPh_4$ gave $[(smif)_2Ir]BPh_4$ (**1**$^+$-Ir). Electrochemical experiments led to the oxidation of **1**-M (M = Cr, Mn, Co) by AgOTf to produce $[(smif)_2M]OTf$ (**1**$^+$-M), and treatment of $Rh_2(O_2CCF_3)_4$ with 4 equiv Na(smif) and 2 AgOTf gave **1**$^+$-Rh. Characterizations by NMR, EPR, and UV−vis spectroscopies, SQUID magnetometry, X-ray crystallography, and DFT calculations are presented. Intraligand (IL) transitions derived from promotion of electrons from the unique CNC^{nb} (nonbonding) orbitals of the smif backbone to ligand π^*-type orbitals are intense ($\varepsilon \approx 10\,000-60\,000$ $M^{-1}cm^{-1}$), dominate the UV−visible spectra, and give crystals a metallic-looking appearance. High energy K-edge spectroscopy was used to show that the smif in **1**-Cr is redox noninnocent, and its electron configuration is best described as (smif(−))(smif(2−))Cr(III); an unusual S = 1 EPR spectrum (X-band) was obtained for **1**-Cr.

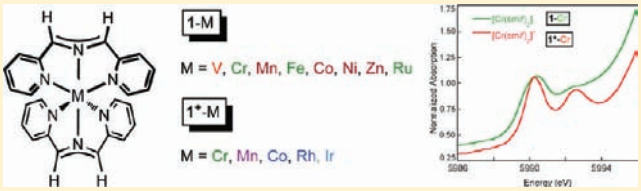

INTRODUCTION

The beginnings of inorganic coordination chemistry can be traced to the laboratories of Alfred Werner,[1] whose archived collection of cobalt complexes at the University of Zurich can still be viewed today with an appropriate request.[2] For a significant part of the 20th century and continuing into the 21st century, investigations into amines and N-donor heterocycles played a dominant role in the field of coordination chemistry, with more attention given to chelates such as bipyridines,[3,4] terpyridines,[5−17] pyrazolyl borates,[18−20] 2-picolyl-amines,[21−27] dipyridylimines and pyridinediimines,[28−32] and bis-(2-pyridylcarbonyl)aminates, among countless others.[33−40] The majority of these compounds contain cationic complex ions, and while first row transition metal (TM) species are prominent, there are plenty of examples containing second and third row TM elements. Even today, one can hardly open a journal with inorganic content and not see a contribution describing the synthesis, characterization or application of a Werner-type coordination compound.

During the course of investigating tetradentate chelate ligands as applied to first row TM elements, a degradation occurred while conducting a metalation reaction with $Cr\{N(TMS)_2\}_2THF_2$.[41,42] As Scheme 1 indicates, a C−N bond was cleaved in the process to yield forest green {1,3-di-(2-pyridyl)-2-azaallyl}$CrN(TMS)_2$, abbreviated as $(smif)CrN(TMS)_2$ (smif = 1,3-di-(2-pyridyl)-2-azaallyl). In the proposed mechanism of its formation,[43] a chromium amide functions as a base, thereby prompting an alternative synthesis from (smif)H, the protonated azaallyl 1,3-di-(2-pyridyl)-2-azapropene, and $Cr\{N(TMS)_2\}_2THF_2$. A related degradation of a di-((2-pyridyl)-CH_2)amide on Zn led to the isolation of the first smif-complex, $(smif)_2Zn$, according to Westerhausen and Kniefel.[44]

Several features of $(smif)CrN(TMS)_2$ were intriguing, especially the optical density of the species, which manifested two intraligand bands of great intensity at 674 nm ($\varepsilon \approx 15\,000$ M^{-1} cm^{-1}) and 396 nm ($\varepsilon \approx 27\,000$ M^{-1} cm^{-1}). The azaallyl unit is also isoelectronic with popular N-heterocyclic carbene ligands,[45−47] as Figure 1 illustrates. Most importantly, due to its monoanionic charge and tridentate capacity, the possibility of

Received: February 22, 2011
Published: November 17, 2011

   dx.doi.org/10.1021/ic200376f | *Inorg. Chem.* 2011, 50, 12414−12436

Scheme 1

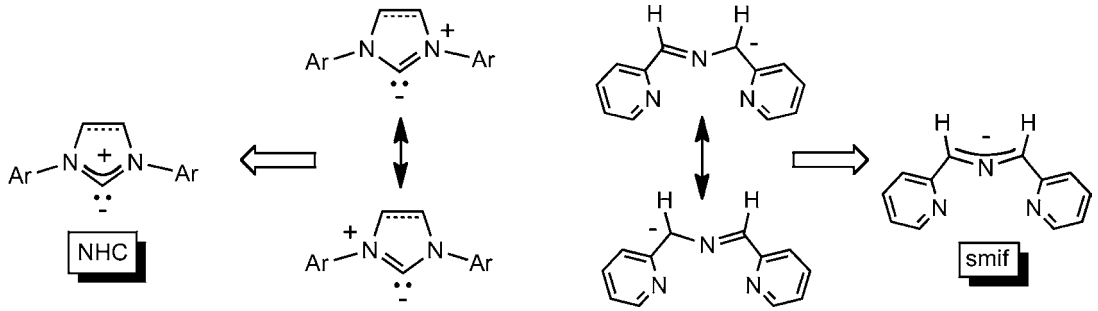

Figure 1. N-Heterocyclic carbenes are isoelectronic with the azaallyl portion of smif.

Scheme 2

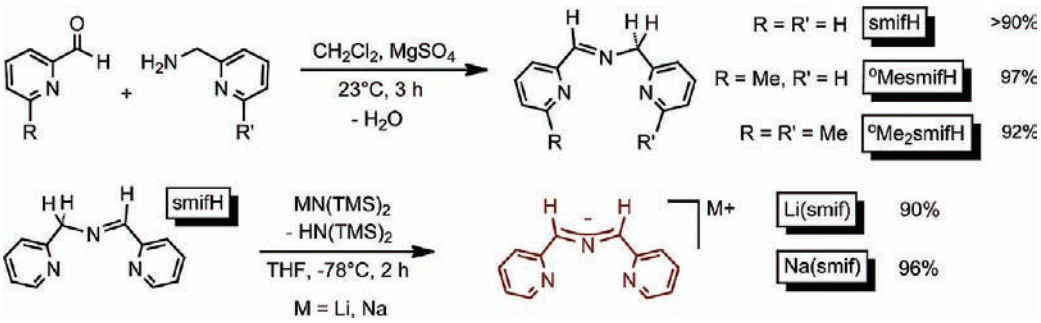

synthesizing Werner-type coordination complexes that were neutral and amenable to study in nonaqueous solvents was appealing. Herein we report the syntheses, characterizations and initial calculations of pseudo-octahedral MN_6 complexes with the composition $(smif)_2M^n$; a few of the derivatives (M = Fe, Co, Co^+, Ni) were previously communicated,[48] and all the complexes described were included in a patent application.[49]

RESULTS

Syntheses. *1. (smif)H and Derivatives.* Condensation of 2-pyridinecarboxaldehyde with 2-(aminomethyl)pyridine afforded 1,3-di-(2-pyridyl)-2-azapropene in >90% yield according to a literature procedure.[50] As shown in Scheme 2, the method was adopted for two methylated species derived from the *o*-methylated pyridine carboxaldehyde and *o*-methylated 2-(aminomethyl)pyridine. One provided a smifH with a methyl group in a single ortho position, that is, ^{o}MesmifH, and the other led to a di-*o*-methylated smif, ^{o}Me$_2$smifH. Deprotonation of smifH was effected with strong bases, and utilization of $LiN(TMS)_2$ and $NaN(TMS)_2$[51] afforded gold crystals of Li(smif) and Na(smif) in excellent yields (≥90%). The alkali metal anions were deep magenta in solution, with bands at 583 ($\varepsilon \approx 18\,000$ M^{-1} cm^{-1}) and 420 nm ($\varepsilon \approx 7000$ M^{-1} cm^{-1}) measured for Li(smif) in benzene.

2. $(smif)_2M$ (M = TM). Neutral $(smif)_2M$ derivatives were prepared via three routes that are illustrated in Scheme 3. The *bis*-amide precursors $M\{N(TMS)_2\}_2THF_n$ (M = Cr, n = 2;[41,42] M = Fe, n = 1)[52] acted as bases when treated with smifH to afford $(smif)_2M$ (**1**-M; M = Cr, Fe) concomitant with 2 equiv $HN(TMS)_2$. This method was also used to prepare di- and tetra-*ortho*-methylated iron derivatives $(^o\text{Mesmif})_2$Fe (**2**-Fe) and $(^o\text{Me}_2\text{smif})_2$Fe (**3**-Fe). While the metal-amide precursor route was considered the cleanest, the requirement of synthesizing various *bis*-amides added a step that was circumvented by standard metathetical procedures with simple metal halides. Typically, Li(smif) was prepared *in situ* from smifH and $LiN(TMS)_2$ at −78 °C in THF (Scheme 2), and the metal halides[53,54] were added and allowed to stir for 16−36 h to afford several $(smif)_2M$ (**1**-M, M = Mn, Fe, Co, Ni, Zn) in reasonable to very good yield. The organometallic precursor $(COD)RuCl_2$[55] and 2 equiv of Na(smif) were used to prepare $(smif)_2Ru$ in similar fashion. Utilization of $Rh_2(O_2CCX_3)_4$ (X = H, F)[56] in metathesis reactions with M′(smif) (M′ = Li, Na) failed to elicit the desired Rh(II) complex, and PdX_2 and PtX_2 sources also failed to produce the corresponding *bis*-smif derivatives, although ample chemistry, especially for Pd, was noted. While the proposed 19 and 20 e^- compounds might not be expected to be stable, the potential for smif to accommodate additional electrons as a redox-active ligand (vide infra) prompted the attempts. Scheme 3 also provides the colors of the $(smif)_2M$ (**1**-M) derivatives and their complementary solid state appearances, which were often gold-bronze (or gold

dx.doi.org/10.1021/ic200376f | Inorg. Chem. 2011, 50, 12414–12436

Scheme 3

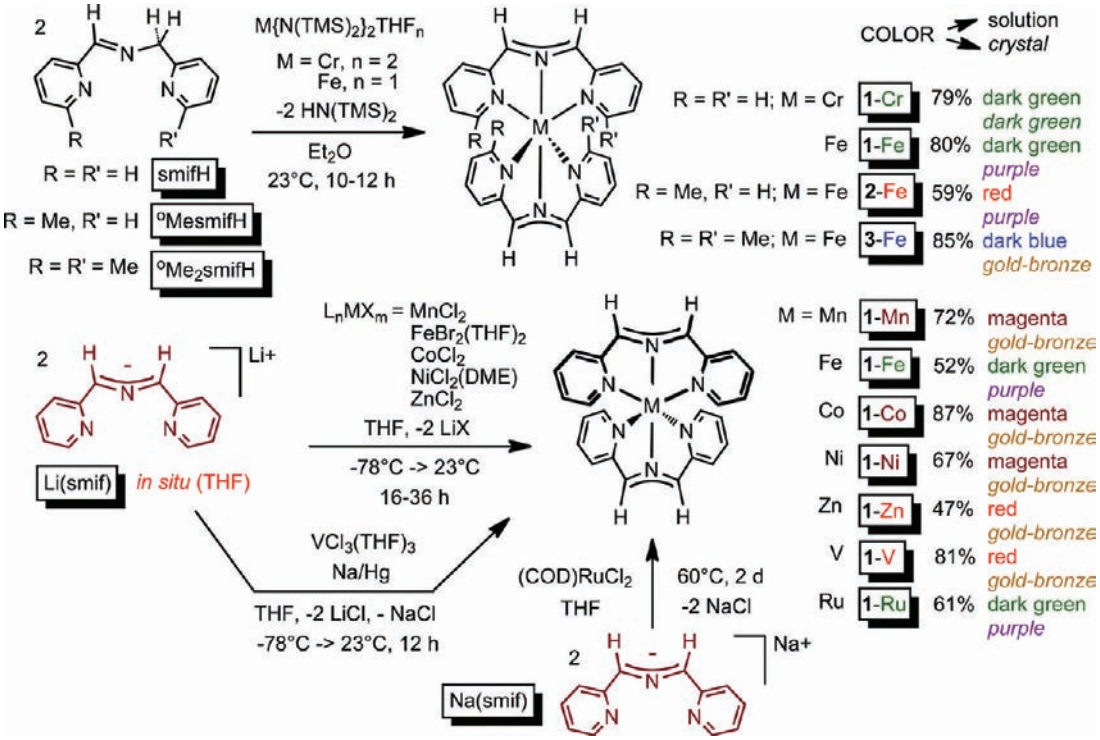

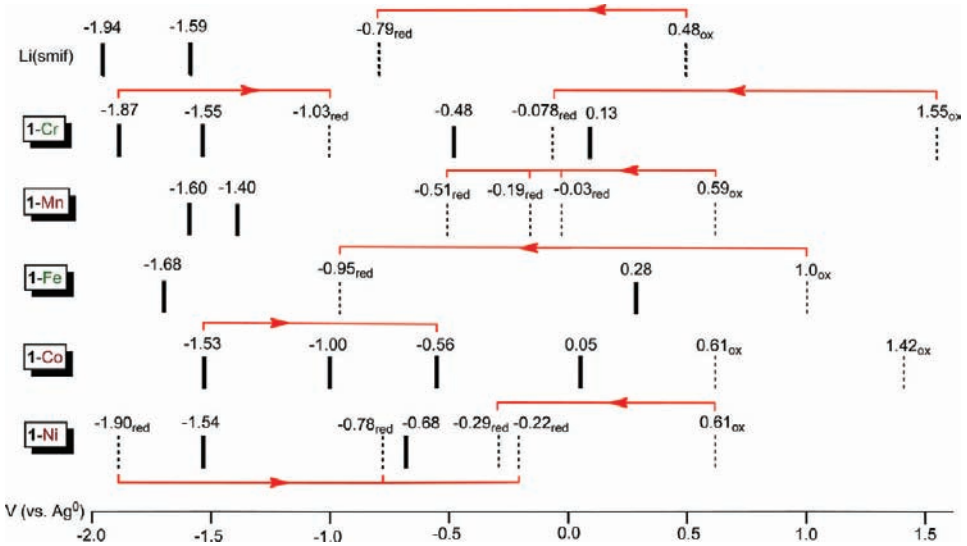

Figure 2. Summary of electrochemical potentials determined from cyclic voltammetry (typically 1 V/s) in THF with ~1 mM **1**-M, 0.1 M TBAP as supporting electrolyte, Pt wire working electrode, and Ag wire as a pseudoreference electrode (approximate to Ag^0/Ag^+ (0.1 M), which is 0.49 V vs SCE; 0.73 V vs NHE). Reversible potentials are shown with a bold line, and irreversible potentials are labeled; origins of irreversible potentials (when identified) are indicated by the red connectivity and arrows.

depending on crystal size) and indicative of reflectivity because of a large absorption in the red region of the visible spectrum.

Completion of the entire series of first row TMs required synthesis of titanium, vanadium, and copper derivatives. While the preparation of other smif-containing titanium species has been realized, the work will be reported in a separate article.[57] Various attempts at preparing $(smif)_2Cu$ failed, and it is suspected that the azaallyl bridge of the complex is too reactive with regard to CC-bond forming processes. Finally, since appropriate V(II) precursors are not common, the combination of 2 equiv Li(smif), 1 equiv of reducing agent (i.e., Na/Hg), and $VCl_3(THF)_3$[58] enabled the synthesis of $(smif)_2V$ in 81% yield.

3. Electrochemistry. Li(smif) and a select group of **1**-M (M = Cr, Mn, Fe, Co, Ni) were subjected to cyclic voltammetry to help determine whether redox processes could be used to synthesize related cations or anions. Note that the neutral character and air-sensitivity of the species limited analyses to THF solutions, in part because acetonitrile proved to react in certain cases. Figure 2 shows a chart summarizing the assay that reveals possible noninnocent redox activity of the smif at high negative potentials (~ −1.6 V vs Ag^0/Ag^+) observed for both

dx.doi.org/10.1021/ic200376f | Inorg. Chem. 2011, 50, 12414–12436

Scheme 4

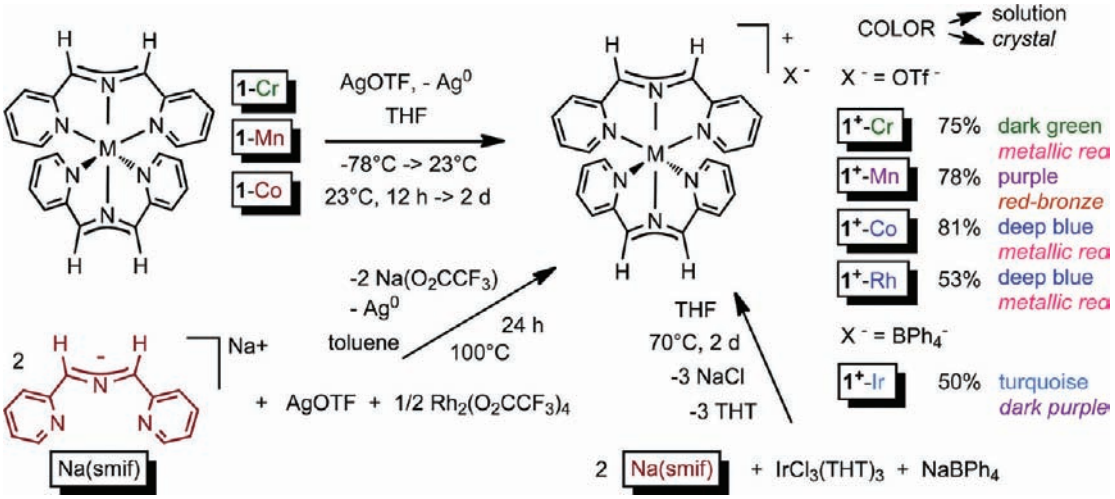

Scheme 5

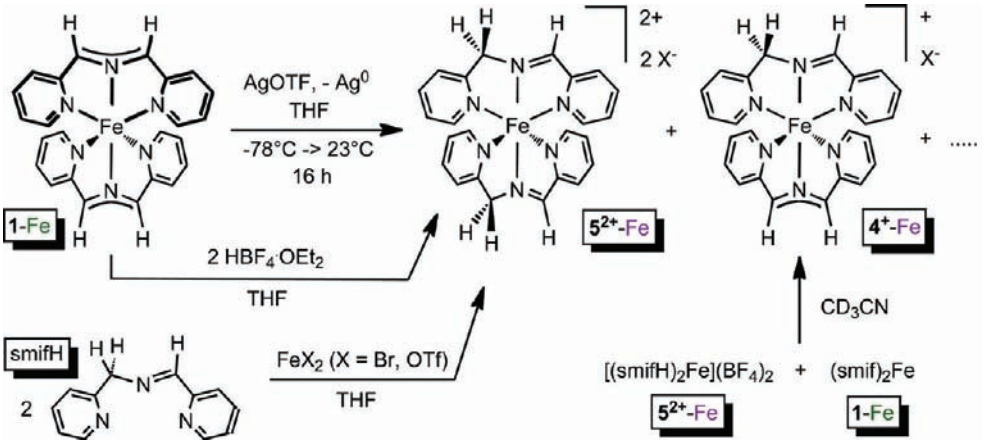

Li(smif) and **1**-M. In general, the electrochemistry of these first row elements is rich, yet the number of irreversible processes, especially those originating from apparent smif reduction, suggests that the reactivity of the system might hamper the isolation of some ions. There is also no clear trend for oxidation, but reversible potentials ≤0.0 V (Ag^0/Ag^+ at ~0.49 V vs SCE) suggested that cations could be prepared from mild oxidants, so reactions with AgOTf were explored.

4. Cations [(smif)$_2$M]$^+$. The redox chemistry observed electrochemically was synthetically scaled with modest success, as indicated in Scheme 4. AgOTf oxidations of (smif)$_2$M (**1**-M; M = Cr, Mn, Co) in THF produced the corresponding cations [(smif)$_2$M]OTf (**1**$^+$-M; M = Cr, Mn, Co) in excellent yields (75−81%). The ready preparation of **1**$^+$-Mn was surprising given the lack of a reversible metal-based couple; however, an oxidation wave at 0.59 V (vs Ag^0/Ag^+) was present, and served as the origin of three irreversible reduction waves. Both (smif)$_2$V (**1**-V) and **1**-Ni yielded intractable brown-black solids when exposed to AgOTf, despite the observation of a reversible couple at −0.68 V (anodic sweep) for the latter. It is plausible that a Ni(III) species was stable on the time scale of the electrochemical experiment (1 V/s), but underwent chemical degradation during the time of a chemical oxidation.

Since neutral second and third row (smif)$_2$M species could not be directly synthesized, with the exception of **1**-Ru, d^6 cations were directly prepared for M$^+$ = Rh(III) and Ir(III). Treatment of $Rh_2(O_2CCF_3)_4$[56] with 2 equiv of Na(smif) in toluene in the presence of AgOTf afforded [(smif)$_2$Rh]OTf (**1**$^+$-Rh) in 53% yield, despite the fact that AgOTf oxidized Na(smif) quite rapidly in a separate experiment. It is plausible that the relative insolubilities of the reagents in toluene result in preferential oxidation of smif-containing Rh species over Na(smif), ultimately leading to the Rh(III) product. A related effort to prepare [(smif)$_2$Cu]$^+$ was unsuccessful. The corresponding Ir(III) compound, [(smif)$_2$Ir]BPh$_4$ (**1**$^+$-Ir), was prepared via metathesis of $IrCl_3(THT)_3$[59] with Na(smif) in the presence of $NaBPh_4$.

Iron derivatives (smif)$_2$Fe (**1**-Fe) and (^{o}Me$_2$smif)$_2$Fe (**3**-Fe) were not successfully oxidized with Ag(I) or other mild oxidants with the necessary potential, and Scheme 5 provides some indication of the fate of the former. Oxidation of **1**-Fe led to a mixture of four products, all containing spectral signatures of smifH; two were identified by independent syntheses as the cation [(smifH)(smif)Fe]OTf (**4**$^+$-Fe) and the dication [(smifH)$_2$Fe](OTF)$_2$ (**5**$^{2+}$-Fe). The addition of 2 equiv smifH to FeX_2 (X = Br, OTf) led to the known dication [(smifH)$_2$Fe]X$_2$ (**5**$^{2+}$-Fe),[28] as did direct diprotonation of **1**-Fe with 2 equiv of HBF_4. Dication **5**$^{2+}$-Fe and **1**-Fe comproportionated to give **4**$^+$-Fe in an NMR tube scale experiment in CD_3CN. If oxidation of **1**-Fe occurred at the ligand, as predicted by calculations (vide infra), it is possible that H-atom abstraction events led to the products containing smifH.

dx.doi.org/10.1021/ic200376f | Inorg. Chem. 2011, 50, 12414–12436

5. Chemical Reductions. All attempts to prepare $[(smif)_2M]^-$ ($\mathbf{1}^-$-M) from the neutral precursors failed, even though varied reaction conditions and a host of reagents were employed. While the electrochemical measurements suggested that smif could harbor an additional electron for all of the complexes, $\mathbf{1}^-$-M must not be stable in the reduction medium or on the time scale of the chemical reduction. Cyclic voltammetry on $[(smif)_2Rh]OTf$ ($\mathbf{1}^+$-Rh) in THF revealed quasi-reversible waves at ~ -1.2 V and ~ -1.6 V and irreversible oxidations at 0.92 and 1.38 V. Attempts to chemically reduce $\mathbf{1}^+$-Rh to form a Rh(II) species that would have a formal smif dianion failed and evidence of free smif anion was observed optically. Related measurements on $[(smif)_2Ir]BPh_4$ ($\mathbf{1}^+$-Ir) in THF showed quasi-reversible waves at -1.18 V and ~ -1.6 V, an irreversible reduction at -0.96 V and an irreversible oxidation at 1.28 V among several minor waves. Again, chemical reductions failed concomitant with the appearance of free smif anion.

Calculations. *1. $(smif)_2Fe$ (1-Fe).* As a guide toward understanding the electronic structures and the unusual optical phenomena affiliated with $(smif)_2M$ (**1**-M; M = V, Cr, Mn, Fe, Co, Ni), density functional (DFT) calculations were conducted. Figure 3 shows a truncated MO diagram for D_{2d} **1**-Fe, chosen

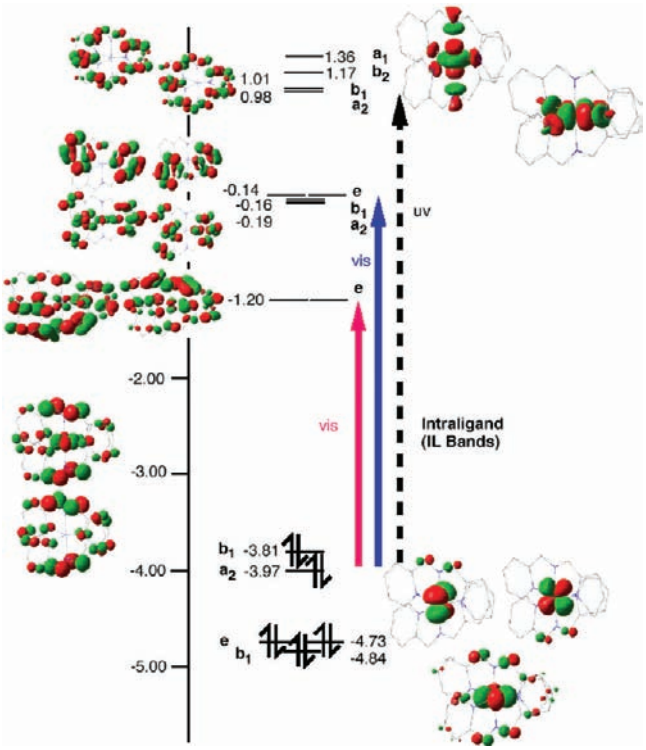

Figure 3. Truncated molecular orbital diagram of $(smif)_2Fe$ (**1**-Fe) showing origin of dominant intraligand bands in red and blue regions of the UV–vis spectrum.

because the electron–electron correlation factors do not complicate this representation since it is a closed-shell system. The HOMO and HOMO-1 orbitals are two linear combinations (b_1 and a_2) of the azaallyl nonbonding orbital containing a node at nitrogen and opposing phase p-orbitals at the two carbons (CNC^{nb}). Roughly 0.9 eV below this set are the e (d_{xz}, d_{yz}) and b_1 (d_{xy}) orbitals of this low spin d^6 complex that are nearly pure d in character. Perhaps the failed oxidation attempts on **1**-Fe resulted from removal of an electron from the ligand HOMO and subsequent reactivity of the ligand radical thus created, providing a rationale for products derived from H-atom abstraction (Scheme 5).

Allowed transitions from the CNC^{nb} orbitals to an e set of ligand π^*orbitals at -1.20 eV transfer charge from the CNC-backbone to the pyridines of the smif, incurring a large electric dipole change ("red" IL bands). A second set of intraligand (IL) transitions from the CNC^{nb} orbitals to a group of ligand π^* orbitals at -0.14 to -0.19 eV also transfers charge from the backbone to the pyridines ("blue" IL bands). Large intensities are expected from IL bands of this type, and this is experimentally observed. The energy differences between filled orbitals and virtual (empty) orbitals should not be construed as accurate, but the relative energies of filled vs filled orbitals, etc., are reasonably accurate,[61,62] hence the IL bands are expected to be roughly 1.0 eV apart.

2. Comparison of $(smif)_2M$ (1-M; M = V, Cr, Mn, Fe, Co, Ni). Because of spin polarization, unrestricted DFT calculations of the "open-shell" systems, that is, $(smif)_2M$ (**1**-M; M = V, Cr, Mn, Co, Ni), can generate alpha and beta spins at different energies and with differing orbital compositions despite population of congeneric spatial orbitals. In Figure 4, energies of the alpha and beta spins of the same orbital parentage have been "averaged" to produce truncated molecular orbital diagrams that can be better visually assessed. This approximation is not without its problems, but there are some clear predictions that can be tested with experiments. In the cases of **1**-Cr, **1**-Mn, and **1**-Co, additional electrons are calculated to reside in smif π^* orbitals, rendering these metals M(III) with the $(smif)_2$ ligands carrying a total of 3– charge. The total spin state is ambiguous in these cases. For example, the calculations of $(smif)_2Mn$ (**1**-Mn) show one electron in $d_{x^2-y^2}$ and one in smif π^*, with a total spin of $S = 3/2$, but computationally the $S = 5/2$ solution is very close in energy, hence the latter spin state was chosen for the diagram in compliance with experiment. That is not the least of the problems with **1**-Mn, as the calculation yields half-filled orbitals lower than filled, and a clear discontinuity in the trends of dπ- and dσ-orbitals relative to **1**-Cr and **1**-Fe. Multireference calculations suggest that this is actually a conventional HS Mn(II) species with a weak-field d^5 configuration above the CNC^{nb} orbitals in energy.[63]

Bis-smif vanadium **1**-V is predicted to be $S = 3/2$, but the HOMO of the system has considerable ligand character (~50% smif π^*), whereas the HOMO of **1**-Cr is clearly smif π^* and contains an electron that is antiferromagnetically (AF) coupled to a Cr(III) $S = 3/2$ center, resulting in a total spin system of $S = 1$. The Co complex **1**-Co is similarly portrayed by the calculations, with its odd electron residing in a smif π^* orbital, and **1**-Ni is calculated to be a standard Ni(II) species with both $d_{x^2-y^2}$ and d_{z^2} singly occupied. It was with these calculations in hand that complementary physical inorganic investigations of **1**-M were conducted, but the inconsistencies prompted higher level computational approaches.[63]

General Structural Features of $(smif)_2M^n$ ($\mathbf{1}^n$-M). Table 1 lists selected data acquisition and refinement details pertaining to $(smif)_2M$ (**1**-M; M = V, Cr, Mn, Fe, Co, Ni) and $[(smif)_2M]OTf$ ($\mathbf{1}^+$-M; M = Cr, Co). Curiously, all of the neutral compounds aside from D_{2d} **1**-Fe crystallized with two molecules in the asymmetric unit, and often a solvent molecule was present; in many cases SQUEEZE was applied during refinement. Since the bite angle formed by the azaalyl nitrogen (N_{aza}) and each pyridine nitrogen (N_{py}) is ~80°, there is considerable space for modest deviations from D_{2d} symmetry,

dx.doi.org/10.1021/ic200376f | Inorg. Chem. 2011, 50, 12414–12436

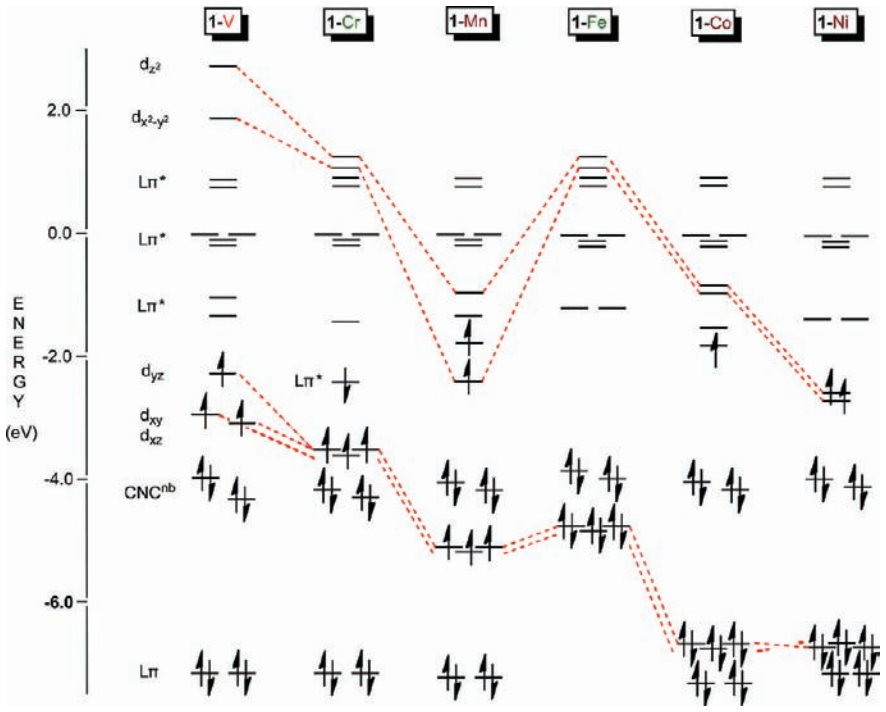

Figure 4. Truncated molecular orbital diagrams for $(smif)_2M$ (**1**-M; M = V, Cr, Mn, Fe, Co, Ni); for comparison to octahedral systems, $d_{x^2-y^2}$ placed on the bond axes. All orbital energies should be considered approximate; for the open shell cases alpha- and β-spins of related orbital parentage were averaged to generate the filled orbital. Dashed red lines correlate the nonbonding d_{xy}, d_{xz}, and d_{yz} set of orbitals and the $d_{x^2-y^2}$ and d_{z^2} set of sigma-antibonding orbitals. The CNC^{nb} orbitals have essentially the same energies independent of metal. Ligand orbitals above the CNC^{nb} pair are primarily pyridine Lπ*, and ligand orbitals below are essentially pyridine π-bonding in character.

and Figure 5 illustrates the types of distortions expected. An axial or propeller twist about the N_{aza}–M–N'_{aza} axis removes the mirror planes and renders the resulting structure D_2, and if pyridines of opposing smif ligands approach one another in addition to the twist, the symmetry is further lowered to C_2. If one smif is pulled away from the metal while the N_{aza}-M-N'_{aza} angle remains 180°, this axial elongation results in C_{2v} symmetry, but if the smif is canted such that $\angle N_{aza}$-M-N'_{aza} is no longer 180°, only a mirror plane remains (C_s).

Pertinent structural parameters for $[(smif)_2M]^n$ (n = 0, **1**-M; n = 1, **1**$^+$-M) are given in Table 2, where they are listed as average values when statistically appropriate. All of the compounds are roughly D_{2d}, with very subtle deviations that render all species except $(smif)_2Fe$ (**1**-Fe) and $[(smif)_2Co]OTf$ (**1**$^+$-Co) rigorously assigned C_1 symmetry. The distortions that best describe the subtle changes from D_{2d} are listed in the table, where the N_{aza}–M–N'_{py} angles and visualization often provided the best means to assess the deviations.

Characterizations. *1. Iron.* Figure 6 illustrates $(smif)_2Fe$ (**1**-Fe), which has a regular D_{2d} structure with no clear distortions, as expected for a low spin d^6 configuration. The azaallyl nitrogen–iron distances average 1.9012(14) Å, which is significantly shorter than the corresponding Fe-py average distance of 1.9634(12) Å. The azaallyl nitrogens are essentially linear about the iron (179.11(6)°), and smif possesses a $N_{aza}FeN_{py}$ bite angle of 82.3(2)°, consistent with tight binding in the low spin complex. Pyridine nitrogens on opposing smif ligands are 91.0(12)° apart, and $N_{aza}FeN'_{py}$ angles average 97.7(5)°. The d(CN) of the azaallyl group is 1.333(3) Å, consistent with significant double bond character.

The diamagnetism observed for $(smif)_2Fe$ (**1**-Fe) is corroborated by the zero field Mössbauer spectrum shown in Figure 7, as previously described,[48] whose δ of 0.30(1) mm/s, modest ΔE_Q of 0.62(1) mm/s, and sharp line width of 0.25(1) mm/s may be construed as typical for low spin Fe(II) complexes with relatively symmetric electron density. Single *o*-Me substitution of the smif ligand, that is, $(^oMesmif)_2Fe$ (**2**-Fe), generates a rather modest change in the Mössbauer spectrum, with a greater ΔE_Q of 0.99 mm/s and an increased line width indicating slightly greater asymmetry in the electron density about the Fe(II) center. A notable change occurs in $(^oMe_2smif)_2Fe$ (**3**-Fe), whose isomer shift (δ = 1.04 mm/s) is now more consistent with a high spin Fe(II) configuration, with a ΔE_Q of 2.18 mm/s that is also typical of an S = 2 iron center.[64]

Five and six resonances are observed in the ^1H and $^{13}C\{^1H\}$ NMR spectra of $(smif)_2Fe$ (**1**-Fe), respectively, with the azaallyl proton at δ 7.59 and its accompanying carbon at δ 112.19. The expected ten resonances were found in the ^1H NMR spectrum of $(^oMesmif)_2Fe$ (**2**-Fe), and while most of the shifts were reasonable, the azaallyl hydrogens were at δ 11.43 and 12.04 with linewidths of 29 and 46 Hz, respectively; furthermore, the C^3H proton of the unsubstituted pyridine was found at δ 13.31 with a line width of 52 Hz. Together, these broad, downfield resonances suggest some paramagnetic character in the sample. The dimethylated smif complex, $(^oMe_2smif)_2Fe$ (**3**-Fe) is characterized by a ^1H NMR spectrum clearly characteristic of a paramagnetic species,[65] with shifts ranging from δ −9.64 ($(CH)_2N$, $\nu_{1/2} \sim 110$ Hz) to δ 167.44 (py-CH, $\nu_{1/2}$ = 53 Hz).

Figure 8 illustrates SQUID magnetic measurements for $(^oMesmif)_2Fe$ (**2**-Fe) and $(^oMe_2smif)_2Fe$ (**3**-Fe) that corroborate the Mössbauer and NMR spectroscopic details above. The dimethylated smif derivative **3**-Fe has a μ_{eff}(298 K) of ~5.5 μ_B from 50 to 300 K indicative of a high spin S = 2 center with significant orbital or spin-orbit contributions,[66,67] as is plausible

dx.doi.org/10.1021/ic200376f | Inorg. Chem. 2011, 50, 12414–12436

Table 1. Selected Crystallographic and Refinement Data for $(smif)_2M$ (1-M; M = V, Cr, Mn, Fe, Co, Ni) and $[(smif)_2M]OTf$ (1^+-M; M = Cr, Co)

	1-V	1-Cr	1^+-Cr	1-Mn
formula	$C_{24}H_{20}N_6V$[a,b]	$C_{24}H_{20}N_6Cr$[a,c]	$C_{29}H_{28}N_6O_4F_3SCr$[d]	$C_{24}H_{20}N_6Mn$[a,c]
formula wt	443.40	444.46	665.63	447.40
space group	$P\bar{1}$	$P\bar{1}$	$P\bar{1}$	$P\bar{1}$ bar
Z	4	4	2	4
a, Å	8.940(6)	8.9763(6)	8.7769(4)	8.9189(11)
b, Å	14.245(9)	14.4378(10)	12.5575(6)	14.4448(19)
c, Å	17.526(9)	16.9883(11)	15.6932(7)	17.849(2)
α, deg	94.41(5)	94.086(4)	86.978(3)	94.240(6)
β, deg	98.06(5)	97.642(4)	76.027(3)	98.287(6)
γ, deg	96.16(4)	97.152(4)	80.361(3)	93.988(5)
V, Å^3	2188(2)	2156.5(3)	1654.63(13)	2261.8(5)
ρ_{calcd}, g·cm^{-3}	1.346	1.369	1.336	1.314
μ, mm^{-1}	0.477	0.554	0.467	0.606
temp, K	100(2)	173(2)	173(2)	296(2)
λ (Å)	0.97890	0.71073	0.71073	0.71073
R indices	R1 = 0.0482	R1 = 0.0484	R1 = 0.0482	R1 = 0.0433
$[I > 2\sigma(I)]$[g,h]	wR2 = 0.1444	wR2 = 0.1008	wR2 = 0.1135	wR2 = 0.0910
R indices	R1 = 0.0500	R1 = 0.0816	R1 = 0.0677	R1 = 0.0754
(all data)[g,h]	wR2 = 0.1469	wR2 = 0.1109	wR2 = 0.1208	wR2 = 0.0997
GOF[i]	1.071	1.034	1.075	1.024
	1-Fe	1-Co	1^+-Co	1-Ni
formula	$C_{24}H_{20}N_6Fe$	$C_{24}H_{20}N_6Co$[a]	$C_{29}H_{28}N_6O_4F_3SCo$[d]	$C_{25.5}H_{21.5}N_6Ni$[f]
formula wt	448.31	451.39	672.56	470.70
space group	$P2_1/n$	$P\bar{1}$	$C2/c$	$P\bar{1}$
Z	4	4	8	4
a, Å	8.7442(4)	9.028(6)	30.8068(12)	9.0129(8)
b, Å	27.4138(14)	14.398(9)	14.4243(5)	14.4774(12)
c, Å	9.2149(4)	16.882(9)	18.5224(7)	17.0517(14)
α, deg	90	93.92(5)	90	94.368(3)
β, deg	113.809(2)	98.35(5)	126.141(2)	97.829(3)
γ, deg	90	97.35(4)	90	97.521(3)
V, Å^3	2020.93(16)	2145(2)	6646.9(4)	2175.2(3)
ρ_{calcd}, g·cm^{-3}	1.473	1.398	1.344	1.437
μ, mm^{-1}	0.771	0.824	0.637	0.918
temp, K	173(2)	100(2)	173(2)	213(2)
λ (Å)	0.71073	0.97890	0.71073	0.71073
R indices	R1 = 0.0424	R1 = 0.0474	R1 = 0.0551	R1 = 0.0436
$[I > 2\sigma(I)]$[g,h]	wR2 = 0.0932	wR2 = 0.1325	wR2 = 0.1424	wR2 = 0.0795
R indices	R1 = 0.0586	R1 = 0.0488	R1 = 0.0782	R1 = 0.0882
(all data)[g,h]	wR2 = 0.1001	wR2 = 0.1349	wR2 = 0.1543	wR2 = 0.0934
GOF[i]	1.041	1.030	1.055	1.004

[a]The asymmetric unit contains two formula units. [b]SQEEZE applied to 1/2 molecule of toluene per asymmetric unit. [c]SQEEZE applied to toluene molecule. [d]The asymmetric unit contains one molecule of 1^+-M and one molecule of THF; SQEEZE was applied to a second THF. [f]The asymmetric unit contains two molecules of 1-Ni and 1/2 molecule of C_6H_6. [g]$R1 = \Sigma||F_o| - |F_c||/\Sigma|F_o|$. [h]$wR2 = [\Sigma w(|F_o| - |F_c|)^2/\Sigma wF_o^2]^{1/2}$. [i]GOF (all data) = $[\Sigma w(|F_o| - |F_c|)^2/(n - p)]^{1/2}$, n = number of independent reflections, p = number of parameters.

for octahedral Fe(II) centers. The downturn in moment below 50 K is a consequence of zero field splitting (ZFS), a combination of spin−orbit coupling and low symmetry effects (JulX fit, see Supporting Information).[66,67] In contrast, $(^oMesmif)_2Fe$ (2-Fe) has a μ_{eff} of 1.22 μ_B at 298 K that declines to ~0.8 μ_B at 30 K. This steady decrease is consistent with temperature independent magnetism (TIP) as a significant factor in the paramagnetism of 2-Fe, and also explains why its NMR and Mössbauer spectra were only slightly changed from that of $(smif)_2Fe$ (1-Fe); the curve is greater than that expected from TIP alone, hence a small amount of paramagnetic impurity (PI, fit as $S = 2$) is likely present (JulX fit (D is the zero field splitting parameters): g = 2.00, $|D| = 0.729$ cm^{-1}, $E/D = 0.137$, TIP = 286 × 10^{-6} emu, PI = 2.7%). TIP arises from mixing of a nearby excited state that is not thermally populated, hence 2-Fe would appear to be on the cusp of changing spin state, yet possesses an $S = 0$ ground state.

The aforementioned data suggests that the moderately strong field imparted by the smif ligands in $(smif)_2Fe$ (1-Fe) is disturbed by single methylation of the ligand in the ortho-positions, but the minor steric change does not disrupt the binding enough to change the spin state. Nonetheless, the methylation has brought an excited state into proximity from an energy standpoint. Dimethylation of the smif is enough to sterically hamper binding and significantly weaken its field strength, thereby incurring a change to the high spin, $S = 2$ ground state found for $(^oMe_2smif)_2Fe$ (3-Fe).

dx.doi.org/10.1021/ic200376f | Inorg. Chem. 2011, 50, 12414–12436

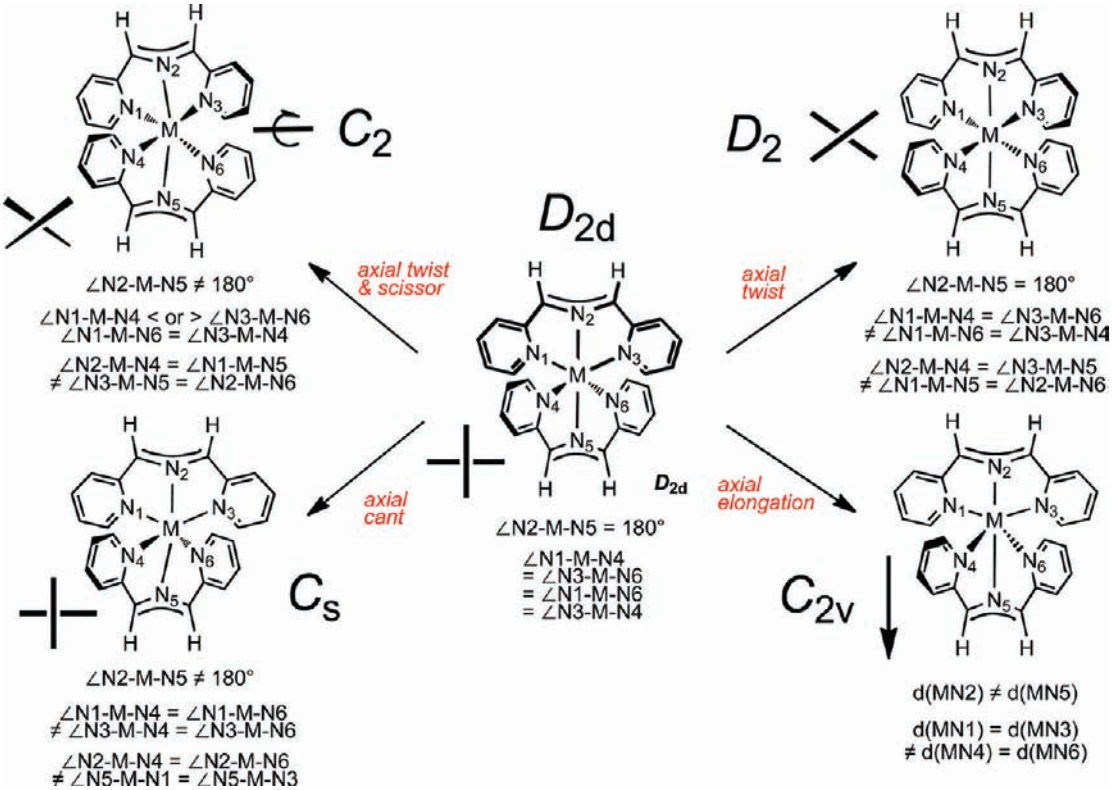

Figure 5. Common structural distortions of $[(smif)_2M]^n$ (n = 0, **1**-M; n = 1, $\mathbf{1}^+$-M).

The structural changes implicated in the characterizations of $(smif)_2Fe$ (**1**-Fe), $(^oMesmif)_2Fe$ (**2**-Fe) and $(^oMe_2smif)_2Fe$ (**3**-Fe) should be corroborated by UV−vis spectroscopy, but there are complications due to the intense intraligand (IL) absorptions intrinsic to the smif ligand. A TDDFT calculation of the spectrum of **1**-Fe (see Supporting Information) was helpful in assessing the bands, although the calculated spectrum was blue-shifted by 0.24−0.39 eV depending on the feature. The origins of the major absorptions were predominantly intraligand (IL) in character, although several contain some MLCT or LMCT character (Figure 9). The major band in **1**-Fe at 603 nm (ε = 17 800 M^{-1} cm^{-1}) is an IL band in which charge is transferred from the smif-CNC^{nb} to smif-π^* orbitals, as are the other major bands at 506 (ε = 19 500 M^{-1} cm^{-1}), 473 (ε = 21 900 M^{-1} cm^{-1}), and 437 nm (ε = 42 000 $M^{-1}cm^{-1}$). Referring to Figure 3, the lowest energy band is illustrated by the "red" transition, whereas the latter absorptions correspond to the "blue" transitions according to orbital origins given by the TDDFT calculation; some metal to ligand charge transfer (MLCT) is also included. The d-d band(s) expected for the distorted octahedral complex are completely dwarfed by the IL features, but are likely to be in the 550 and 400 nm regions according the calculations, and Δ_{oct} is estimated to be ~18 000 cm^{-1} with an accompanying B of ~470 cm^{-1} from Tanabe-Sugano fits of calculated bands adjusted for the blue shift. Both values are consistent with a relatively covalent complex implicated by its diamagnetism and Mössbauer parameters.

There are two potential "red" IL bands according to Figure 3 ($a_2^2b_1^2 \rightarrow a_2^2b_1^1e^1$, $^1A_1 \rightarrow {}^1E$; $a_2^2b_1^2 \rightarrow a_2^1b_1^2e^1$, $^1A_1 \rightarrow {}^1E$), but the TDDFT calculation shows only one band. The band at 560 nm (ε = 15 600 $M^{-1}cm^{-1}$) is not accounted for by the TDDFT and may be the ν_{GS} = 0 to ν_{ES} = 1 vibrational component affiliated with the 603 nm (ν_{GS} = 0 to ν_{ES} = 0) band.[68,69] It is also possible the 645, 603, and 560 nm bands are the ν_{GS} = 0 to ν_{ES} = 0, 1, and 2 vibrational components, provided the ES potential energy surface is substantially displaced from the GS. The difference of ~1250 cm^{-1} is comparable to ground state IR absorptions that are assigned to the CNC linkage, and it is likely that related excited state features are at similar energies. Related explanations of features observed for mono-smif compounds have been made.[43] The band at 263 nm is another IL band ("black-hashed" in Figure 3), and the low energy features at 885 nm and 790 nm are likely to be triplet components of the IL bands.[70] Their substantial intensities (ε = 2500 M^{-1} cm^{-1}) may be a function of how much the iron mediates spin−orbit coupling, thereby relaxing the forbidden character to the transitions.

o-Methylation of the smif in $(^oMesmif)_2Fe$ (**2**-Fe) causes a blue shift in the IL bands and lends credence to the possibility that the "red IL band" reveals a distinct structural change in the ES, provided the absorptions at 630, 580, and 530 nm are vibrational components. The spectrum also shows an increase in intensity of the "red IL band", and features present in **1**-Fe at ~500 nm are lost, perhaps in accordance with the spectral changes of the main IL bands. Dimethylation of the smif in high spin $(^oMe_2smif)_2Fe$ (**3**-Fe) affords major changes. The "red IL band" has increased in intensity to 58 000 M^{-1} cm^{-1} while the major "blue IL band" decreased to 32 000 M^{-1} cm^{-1}. The origin of the intensity change is not clear, but the change in profile suggests that the ES pertaining to the "red IL band" is not as displaced relative to the GS as in **1**-Fe and **2**-Fe, providing a reason for the intensity gain. Note that the low energy features are diminished (850 nm, 1030 nm ($\varepsilon \approx$ 500 M^{-1} cm^{-1})) in **3**-Fe, suggesting that the S = 2 center is less effective at helping relax the selection rules that permit observation of spin forbidden IL bands.

dx.doi.org/10.1021/ic200376f | Inorg. Chem. 2011, 50, 12414−12436

Table 2. Selected Distances (Å) and Angles (deg)[a] for $[(smif)_2M]^n$ (n = 0, 1-M, M = V, Cr, Mn, Fe, Co, Ni; n = 1, 1^+-M, M = Cr, Co), Point Group, and Closest Identifiable Distortion according to Figure 6

cmpd	d(M−N_{aza})	d(M−N_{py})	d(N_{aza}−C)	∠N_{aza}−M−N'_{aza}	∠N_{py}−M−N_{py}	∠N_{aza}−M−N_{py}	∠N_{aza}−M−N'_{py}	∠N_{py}−M−N'_{py}	Pt Gp	dist
1-V	2.058(18)	2.118(7)	1.347(11)	172.1(4)	154.2(5)	77.3(2)	95.08(10)−110.10(10)	92.8(13)	C_1	C_s
1-Cr	1.9481(19)[b]	2.035(12)	1.341(11)	175.81(18)[b]	158.2(8)	79.2(3)	97.10(8)−104.79(8)[b]	89.36(8)−94.12(8)[b]	C_1	C_{2v}, C_s
	1.992(2)[b]									
	2.026(2)[c]			176.45(8)[c]			97.55(8)−103.37(8)[c]	90.32(8)−94.90(8)[c]		
	1.932(2)[c]									
1$^+$-Cr	1.994(3)	2.035(2)	1.334(2)	176.72(9)	160.79(10)	80.46(8)	97.02(9)−102.13(9)	89.91(9)−92.25(9)	C_1	C_2
1-Mn	2.186(3)[b]	2.235(7)	1.325(5)	169.22(10)[b]	148.6(8)[b]	74.4(3)[b]	95.99(9)−115.16(9)	92.97(9)−97.26(9)	C_1	C_s, C_2
	2.207(2)[b]									
	2.215(2)[c]			166.51(9)[c]	146.7(5)[c]	73.7(2)[b]				
	2.220(3)[c]									
1-Fe	1.9012(14)	1.9634(12)	1.333(3)	179.11(6)	164.53(11)	82.3(2)	97.7(5)	91.0(12)	D_{2d}	none
1-Co[b,d]	1.946(3)	2.193(3), 2.175(3)	1.341(2)	177.30(11)	158.43(11)	79.2(3)	95.12(12)−101.22(12)	91.5(14)	C_1	C_{2v}, C_s
	1.888(3)	1.980(3), 1.962(3)		164.32(12)		82.2(2)				
c,*d*	1.945(3)	2.094(3), 2.116(3)	1.333(9)	177.76(12)	159.78(12)	80.3(6)	97.51(12)−102.12(13)	91.7(24)	C_1	C_2
	1.939(3)	2.049(3), 2.056(3)		160.87(12)						
1$^+$-Co	1.8768(11)	1.9252(19)	1.331(9)	179.05(10)	167.68(9)	83.9(2)	96.1(7)	90.7(19)	D_{2d}	none
1-Ni	2.019(5)	2.093(9)	1.325(4)	176.07(12)	158.1(4)	79.1(3)	96.66(11)−104.63(11)	92.1(16)	C_1	C_2, C_s

[a]Distances and angles were averaged where statistically appropriate; primes indicate atoms on the opposite smif. For **1**-M (M = V, Cr, Mn, Co, Ni), there are two molecules of $(smif)_2M$ per asymmetric unit. [b]Molecule 1. [c]Molecule 2. [d]Molecules 1 and 2 are structurally different.

dx.doi.org/10.1021/ic200376f |*Inorg. Chem.* 2011, 50, 12414–12436

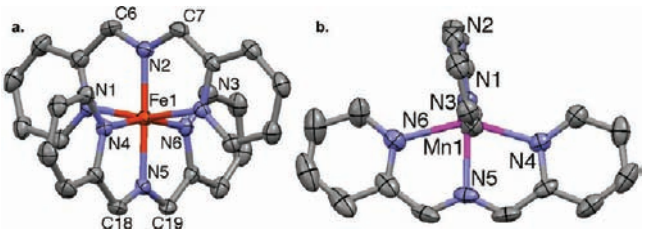

Figure 6. A molecular view of D_{2d} $(smif)_2Fe$ (**1**-Fe, **a.**), and one of $(smif)_2Mn$ (**1**-Mn, **b.**) that illustrates a C_s distortion.

2. Vanadium. The structure of $(smif)_2V$ (**1**-V) has a significant C_s distortion (with slight C_2 twist) observed in the $N_{aza}VN'_{aza}$ angle of 172.1(4)° and varied $N_{aza}VN'_{py}$ angles (95.08(10)-110.10(10)°). The d(VN_{aza}) distance of 2.058(18) Å is 0.15 Å longer than those of **1**-Fe, consistent with the greater covalent radius of vanadium coupled with its low valent V(II) center. The d(VN_{py}) distances of 2.118(7) Å are similarly longer, and the $N_{aza}VN'_{py}$ bite angle is diminished to 77.3(2) as the smif is farther off the metal.

A quartet ground state was calculated for $(smif)_2V$ (**1**-V), and the EPR spectrum shown in Figure 10, taken at 6 K in toluene glass, was consistent with a rhombic $S = 3/2$ spin system, albeit with a small E/D of 0.05(2). An 8-line hyperfine coupling to ^{51}V (I = 7/2, 99.76%) of ∼150 MHz was found for the forbidden transition ($M_s = -3/2 \rightarrow M_s = 3/2$). Figure 11 illustrates a plot of SQUID magnetometry data for **1**-V that shows a μ_{eff} of 3.76 μ_B at 300 K which remains fairly constant until 50 K, when the effects of ZFS are evident; the data are readily fit with the EPR parameters (See Supporting Information). Evans' method solution studies[71] afforded a μ_{eff} of 3.2 μ_B, and while both solid state and solution values are somewhat lower than the spin-only value of 3.87 μ_B, some attenuation due to spin−orbit coupling is normal.[66,67]

The UV−vis spectrum of $(smif)_2V$ (**1**-V) is shown in Figure 12 with the spectra of the iron and chromium derivatives, and while its greatest absorptions range from ∼8000−12 000 M^{-1} cm^{-1}, they are clearly diminished with respect to iron, and significant changes are apparent. The visible region of the spectrum is essentially covered from its UV limit to ∼600 nm by a mélange of bands that are presumably IL or CT in origin. From the calculations in Figure 3, MLCT bands are expected at a lower energy than the lowest IL band, yet the spectrum is

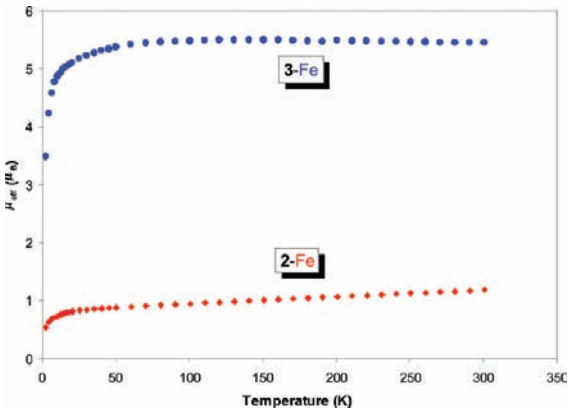

Figure 8. SQUID data (1 T) for $(^oMesmif)_2Fe$ (**2**-Fe) and $(^oMe_2smif)_2Fe$ (**3**-Fe); μ_{eff}(298K) = 1.22 μ_B for **2**-Fe and μ_{eff}(298K) = 5.47 μ_B for **3**-Fe. $(smif)_2Fe$ (**1**-Fe) is diamagnetic.

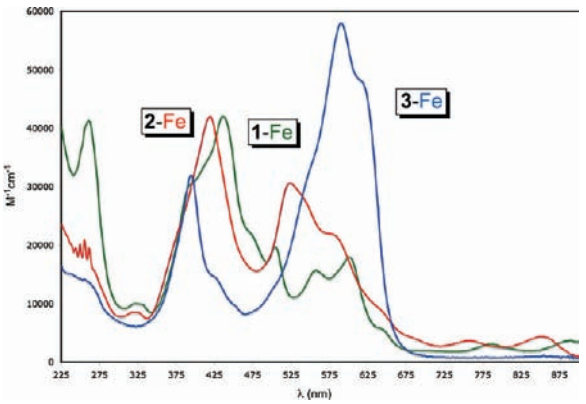

Figure 9. UV−vis spectra for $(smif)_2Fe$ (**1**-Fe, green), $(^oMesmif)_2Fe$ (**2**-Fe, red), and $(^oMe_2smif)_2Fe$ (**3**-Fe, blue) in pentane.

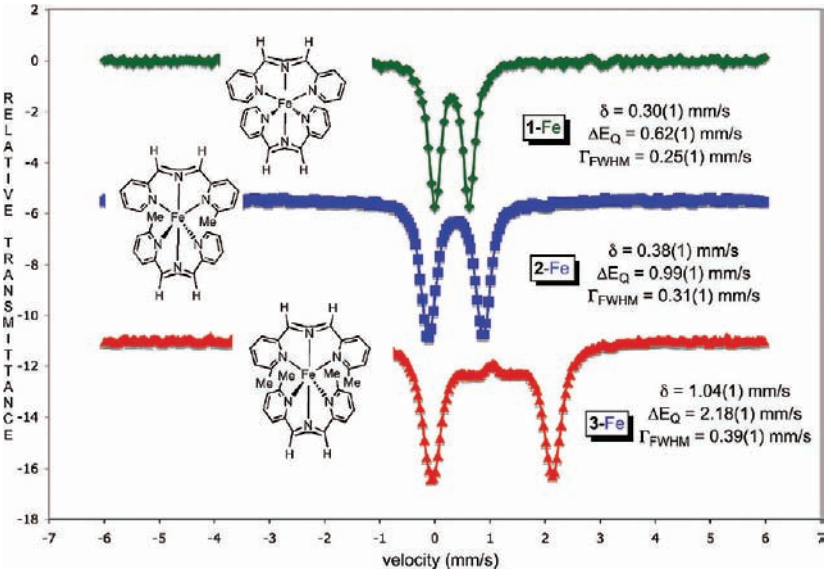

Figure 7. Zero field Mössbauer spectra of $(smif)_2Fe$ (**1**-Fe), $(^oMesmif)_2Fe$ (**2**-Fe) and $(^oMe_2smif)_2Fe$ (**3**-Fe) taken at 80 K. Spectra of **3**-Fe contain variable amounts (∼10−20%) of an unidentified impurity (δ = 1.02 mm/s, ΔE_Q = 0.65 mm/s, Γ_{FWHM} = 0.50 mm/s) that was a component of the fit.

dx.doi.org/10.1021/ic200376f | Inorg. Chem. 2011, 50, 12414−12436

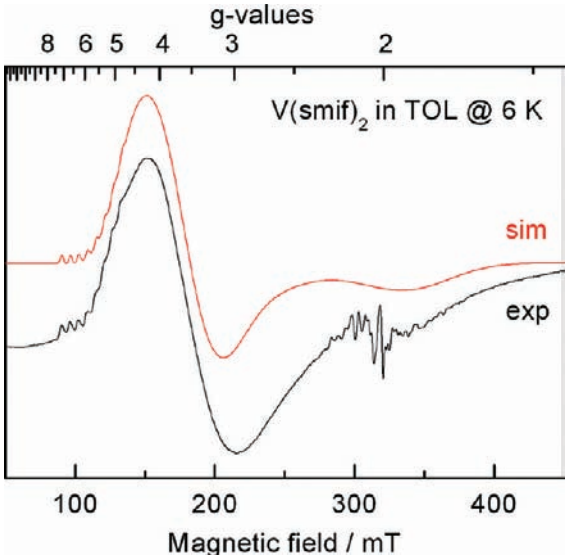

Figure 10. EPR spectrum ($d\chi''/dB$) of $(smif)_2V$ (**1**-V) at 6 K, showing g = 5.67 (forbidden line, $I(V) = 7/2$, $A \approx 150$ MHz (5.00×10^{-3} cm^{-1}), 3.82 and 1.92 lines. Simulation of the spectrum was performed with $S = 3/2$: $g_x = g_y = 1.92$, $g_z = 1.91$; $|D| = 2.6$ cm^{-1}; $E/D = 0.05$. The signals containing hyperfines centered at $g = 2.0$ are likely because of a trace V(IV) impurity.

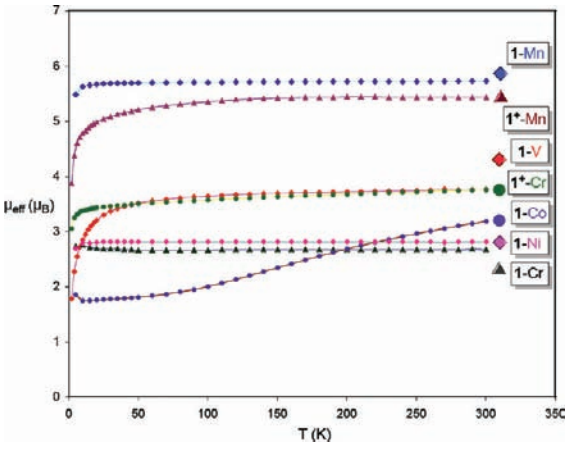

Figure 11. SQUID magnetometry data (1 T) for $(smif)_2M$ (**1**-M; M = V, Cr, Mn, Co, Ni) and $[(smif)_2M]OTf$ ($\mathbf{1}^+$-M; M = Cr, Mn); sight lines are **not** data fits. For JulX fits, see Supporting Information.

surprisingly devoid of features from ~600 nm to broad, lower intensity bands ($\varepsilon \approx 2{,}000$ $M^{-1}cm^{-1}$) at 870 and 950 nm. Similar absorptions appear in most other $(smif)_2M$ (**1**-M), and these appear to be "spin-forbidden" transitions affiliated with the IL bands. Bands at 468 and 397 nm can be considered plausible "blue IL" components according to Figure 3, but the apparent blue shift of the "red IL" band is puzzling, unless the ES of **1**-V is displaced significantly from its GS geometry.

3. Chromium. The two $(smif)_2Cr$ (**1**-Cr) molecules in the asymmetric unit are quite similar, with both exhibiting C_{2v} distortions as the major deviation from D_{2d}. Axial nitrogen distances of 1.992(2) and 2.026(2) Å are significantly longer than their counterparts of 1.9481(19) and 1.932(2) Å, respectively, yet both axial distances are shorter than the pyridine-nitrogen distances of 2.035(12) Å. A subtle lean of one smif relative to the other ($\angle N_{aza}CrN_{aza}$ = 175.81(18)°, 176.45(8)°) characterizes a secondary C_s distortion, which is also evident in the $N_{aza}CrN'_{py}$ and $N_{py}CrN'_{py}$ angles.

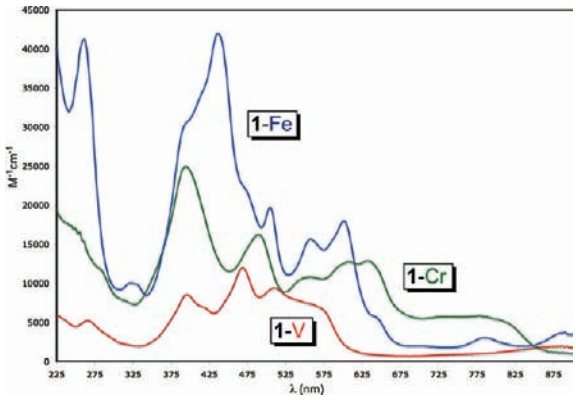

Figure 12. UV–vis spectra of $(smif)_2M$ (**1**-M; M = V, Cr, Fe) in pentane.

Solution studies (Evans' method)[71] and SQUID magnetometry data for $(smif)_2Cr$ (**1**-Cr) gave μ_{eff} of 2.67 μ_B at 300 K, consistent with the expected $S = 1$ ground state for a Cr(II) derivative. In particular, the temperature dependence of μ_{eff} was remarkably flat to 10 K, and the slight upturn at 5 K (1 T, Figure 11) was not evident in data acquired at 3 and 5 T; it may be due to a weak intermolecular interaction (JulX fit $\theta = 0.393$ K). In D_{2d} symmetry the d_{xy} (b_2) and d_{xz},d_{yz} (e) orbitals are intrinsically different, and ZFS from the expected $(b_2)^2(e)^2$ GS configuration mixing with appropriate excited states should be modest, but substantial structural deviations were observed in the solid state. The $|D| \ll 1$ cm^{-1} was thus quite unexpected, and perhaps indicative of an unusual electronic configuration.

EPR spectra were obtained for the $S = 1$ system, and since the $|D|$ values for triplet systems often do not permit observation of signals on standard X-band spectrometers (e.g., for 9 GHz; systems with $|D| > 0.30$ cm^{-1} not observable), care was taken to ensure that the samples were not compromised. Five sets of variable temperature EPR data were obtained on three different samples, and all were identical. Furthermore, temperature-dependent spectral changes were verified for two data sets (i.e., reproducible spectra upon cooling–heating–cooling, etc.), and a spin-counting experiment showed the signal to be 65% (relative to $CuSO_4$) of that expected, a reasonable value. Comparative spectra of $[(smif)_2Cr]OTf$ ($\mathbf{1}^+$-Cr) ruled out the possibility of an impurity due to a simple one electron oxidation.

Spectra of $(smif)_2Cr$ (**1**-Cr) taken in toluene glass at 10 K and in solution at 296 K are given in Figure 13. Simulation of the low temperature spectrum was achieved with "D" = 0.00435 cm^{-1} (E/D = 0.276), and a fit obtained at 296 K possessed similarly small values ("D" = 0.0029 cm^{-1}, $E/D = 0.1$); the parameters were successfully used to fit the SQUID data. Half field signals are often diagnostic of $S = 1$ systems, but in the limit of $D = 0$, the intensity of the forbidden transition diminishes, and in this instance small signals in the $g \approx 4$ region were more consistent with common trace Fe impurities. Furthermore, "D" should not be observed in fluid solution, as the anisotropic part should average out in solution; note that some of the anisotropy is gone in fluid solution, and the spectra were still fit because the "D" in this case is a phenomenological one. In the absence of evidence pertaining to impurities, the reproducible, phenomenological "D" may signify a system where a ligand $S = 1/2$ component is mapped onto a Cr(III) $S = 3/2$ environment, that is, an $S = 3/2$ antiferromagnetically

dx.doi.org/10.1021/ic200376f | Inorg. Chem. 2011, 50, 12414–12436

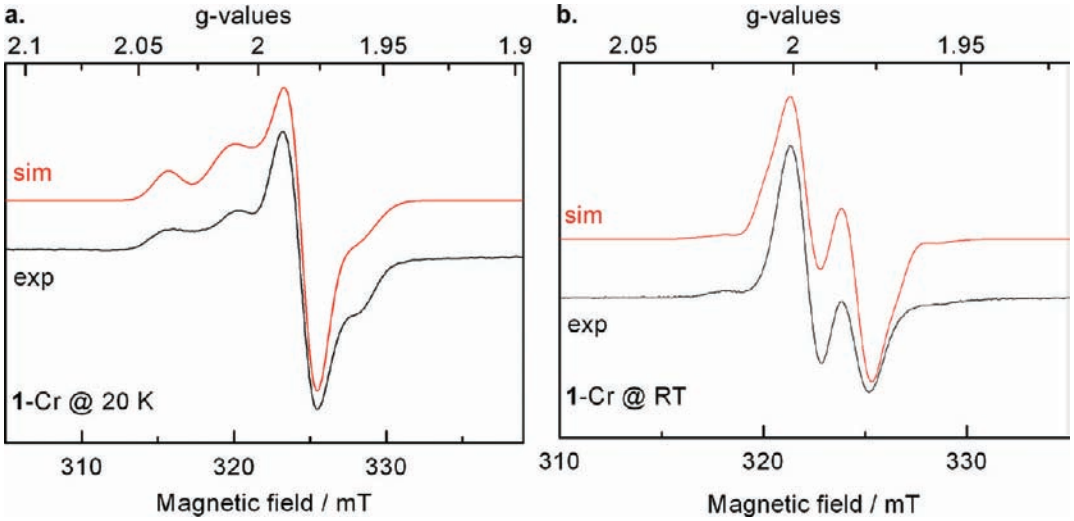

Figure 13. Observed and simulated (red) EPR spectra (dχ''/dB) in toluene of $(smif)_2Cr$ (**1**-Cr) taken at 20 K in a toluene matrix (a, simulation parameters: $S = 1$, $g_x = 1.979$, $g_y = 1.985$, $g_z = 2.007$, "D" = 0.00435 cm^{-1}, $E/D = 0.276$) and in solution at 296 K (b, simulation parameters: $S = 1$, $g_{iso} = 1.9885$, "D" = 0.0029 cm^{-1}, $E/D = 0.1$); in both cases 9.5% of ^{53}Cr ($I = 3/2$, $A_{iso} = 60$ MHz (2.0×10^{-3} cm^{-1}) was taken into account in the simulations. The spectral changes were shown to be reversible. The observed "D" is a phenomenological observable (see text and Supporting Information).

coupled to an $S = 1/2$ system does not necessarily have the spectral signature of an $S = 1$ system. Unfortunately, the expertise necessary to fully understand and vet the spin-Hamiltonian for this system is lacking in this group, but hopefully this phenomenological view of the system will interest others. The data is nonetheless consistent with a ground state that is (smif(−))(smif(2−))Cr(III), in line with K-edge X-ray absorption spectroscopic measurements described below.

The UV−vis spectrum (Figure 12) of $(smif)_2Cr$ (**1**-Cr) is fairly similar to the iron derivative from ∼650 nm to high energies, with the "red IL" band spanning the region from 530 to 650 nm (632 nm, $\varepsilon \approx 12\,900$ M^{-1} cm^{-1}), and a "blue IL" band at 394 nm ($\varepsilon \approx 25\,000$ M^{-1} cm^{-1}); a similar feature at 489 nm ($\varepsilon \approx 16\,300$ M^{-1} cm^{-1}) is likely to be an MLCT band or another "blue IL" band. Below 650 nm is a relatively flat region ($\varepsilon \approx 6\,000$ M^{-1} cm^{-1}) extending to ∼850 nm that is unique to the set of $(smif)_2M$ (**1**-M) in this study. If **1**-Cr is reconfigured as (smif(−))(smif(2−))Cr(III), the absorptions in this region may be assigned as ligand to metal charge transfer (LMCT) bands, but the lack of related absorptions in $(smif)_2V$ (**1**-V) suggests an alternative. Redox noninnocent ligands[72−81] with radical character often exhibit ligand−ligand charge transfer (LLCT) or ligand−ligand intervalence charge transfer (IVCT) transitions,[72−76] and the bands in **1**-Cr may fall in the latter category, although their modest intensities belie such an assignment. A flat region of $\varepsilon \approx 1000$ M^{-1} cm^{-1} extends from ∼900−1150 nm that presumably encompasses triplet features affiliated with the IL bands.

The X-ray crystal structure of $[(smif)_2Cr]OTf$ (**1**$^+$-Cr) revealed the cation to be much more symmetric than $(smif)_2Cr$ (**1**-Cr), with only a modest C_2 distortion revealed by slightly varying $N_{aza}CrN'_{py}$ angles (97.02(9)−102.13(9)°), and an $N_{aza}CrN'_{aza}$ angle of 176.72(9)°. The $d(CrN_{aza})$ distances that average 1.994(3) Å are actually slightly longer than the average distances affiliated with **1**-Cr (1.975(42) Å), perhaps because of diminished overlaps for Cr(III), but the real surprise is how similar they are. The chromium pyridine distances are identical at 2.035(2) Å. In high spin Cr(II)/Cr(III) comparisons, the chromous species is often 0.1−0.2 Å larger in d(CrL). These similarities are consistent with the low spin character attributed to **1**-Cr, but may also be indicative of noninnocent behavior of the smif ligands.

For comparison, the cation $[(smif)_2Cr]OTf$ (**1**$^+$-Cr) was also examined via SQUID magnetometry and EPR spectroscopy. As Figure 12 illustrates, **1**$^+$-Cr manifests a μ_{eff} of 3.76 μ_B at 300 K, and a modest amount of ZFS revealed at temperatures less than 25 K (JulX $g = 2.050$, $D = -0.003$ cm^{-1}, $E/D = 0$, TIP = 1768×10^{-6} emu, $\theta = -0.415$ K). Some attenuation of the spin only value of 3.87 μ_B is common for Cr(III) in octahedral complexes,[66,67] and it is not unreasonable for it to be slightly more pronounced in D_{2d}. Its EPR spectrum is rather featureless (see Supporting Information), but consistent with a symmetric $S = 3/2$ center.

The UV−vis spectrum of $[(smif)_2Cr]OTf$ (**1**$^+$-Cr) is illustrated in Figure 14 along with the other cations in the

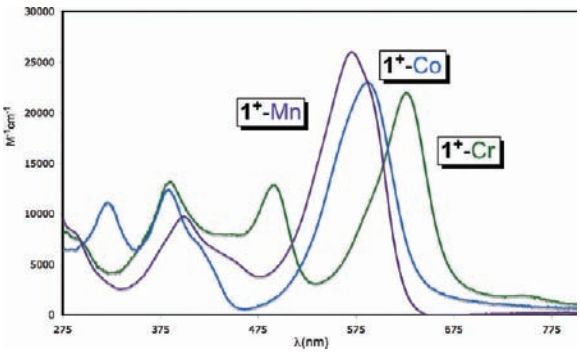

Figure 14. UV−vis spectra of cations $[(smif)_2Cr]OTf$ (**1**$^+$-Cr), $[(smif)_2Mn]OTf$ (**1**$^+$-Mn), and $[(smif)_2Co]OTf$ (**1**$^+$-Co) in THF.

system, and while it is significantly different than $(smif)_2Cr$ (**1**-Cr) in terms of intensity, the main IL bands have a distinct correspondence to the neutral species. The "red IL" band at 626 nm ($\varepsilon \approx 22\,000$ M^{-1} cm^{-1}) is the most intense, and it is slightly blue-shifted from **1**-Cr, with a modest shoulder at ∼583 nm that could be a second red IL band or a vibrational component. The band shape and lack of an obvious vibrational

dx.doi.org/10.1021/ic200376f | Inorg. Chem. 2011, 50, 12414−12436

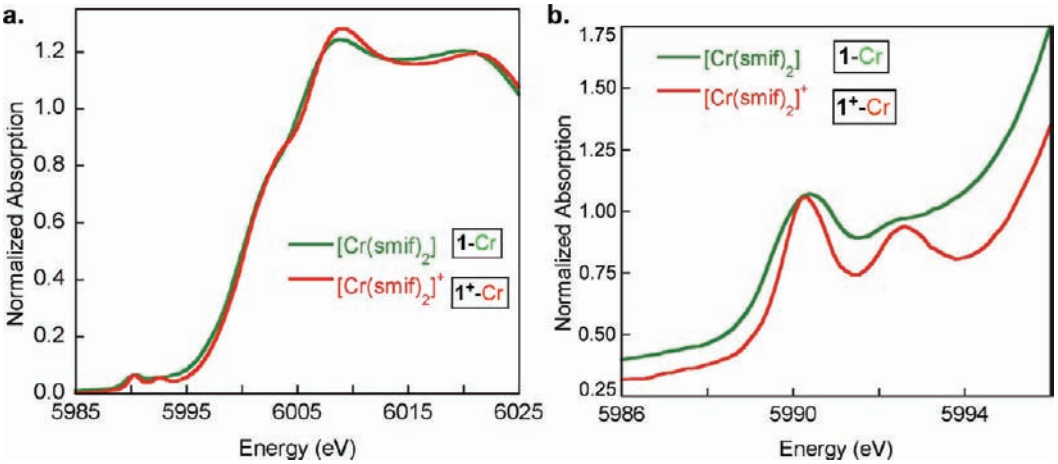

Figure 15. (a) Normalized Cr K-edge spectra (10 K) for $(smif)_2Cr$ (**1**-Cr) and $[(smif)_2Cr]OTf$ (**1**$^+$-Cr). (b) Expanded Cr K-pre-edge region showing 1s → $3d_{xz}/3d_{yz}$ and higher energy 1s → $3d_{x^2-y^2}$ transitions.

progression is consistent with the low amount of distortion in **1**$^+$-Cr relative to its IL excited state. A "blue IL" band is clearly evident at 385 nm ($\varepsilon \approx 13\,200$ M^{-1} cm^{-1}), but the band at 491 nm ($\varepsilon \approx 12\,900$ M^{-1} cm^{-1}) may be an MLCT feature or another IL band. A low energy feature at 741 nm is again likely to be a triplet absorption associated with an IL band.

In view of the structural similarities in $(smif)_2Cr$ (**1**-Cr) and $[(smif)_2Cr]OTf$ (**1**$^+$-Cr), the unusually small D found in the EPR spectra and SQUID data of $(smif)_2Cr$ (**1**-Cr), and the correspondence in band maxima of their respective UV−vis spectra, it is prudent to recognize that calculations suggested **1**-Cr is best formulated as (smif(−))(smif(2−))Cr(III), that is, the smif ligand is noninnocent[72−81] in its ability to accommodate excess charge. High-energy spectroscopies, in particular K-edge spectroscopy, have proven to be useful in discerning the effective charge at metal centers when appropriate models are available.[82−84] As Figure 15 reveals, comparison of the normalized Cr K-edge spectra for **1**-Cr and **1**$^+$-Cr indicates a similar effective nuclear charge for both species, indicative of a ligand-based oxidation process pertaining to removal of an electron from smif(2−). Both compounds exhibit 1s → $3d_{xz}/3d_{yz}$ and 1s → $3d_{x^2-y^2}$ transitions (confirmed by calculations) at roughly the same energies, and the crude Δ_{oct} of 17 500−19 500 cm^{-1} obtained from their difference is a reasonable field strength commensurate with the structural parameters. As suggested by the calculations, the ground state of **1**-Cr appears to be a Cr(III) $S = 3/2$ center antiferromagnetically coupled to a smif $S = 1/2$ center.

4. Manganese. Given the likelihood of $(smif)_2Mn$ (**1**-Mn) being high spin, its distorted structure was not surprising, since longer bond lengths affiliated with weaker Mn-smif binding and the modest bite-angle of smif enable deviations from D_{2d} to be energetically feasible. Figure 6b illustrates the C_s distortion in **1**-Mn, and a secondary C_2 twist is also present. The N_{aza}−Mn distances in the two independent molecules ranged from 2.186(3) to 2.220(3) Å and were accompanied by N_{aza}−Mn−N'_{aza} angles of 169.22(10)° and 166.51(9)°, while the Mn−N_{py} distances were the longest of the neutral derivatives at 2.235(7) Å. The scale of the distortions is most evident in the ∼19° spread in $N_{aza}MnN'_{py}$ angles.

$(smif)_2Mn$ (**1**-Mn) is an $S = 5/2$ molecule, as the SQUID magnetometry data in Figure 11 indicates. The μ_{eff} at 300 K is 5.73 μ_B, very near the expected 5.9 μ_B for a spin-only system, and little ZFS evident (JulX $g = 2.03$, $D = 1.00$ cm^{-1}, $E/D = 0.250$). A broad featured EPR spectrum (see Supporting Information) of **1**-Mn obtained at 8 K was consistent with an $S = 5/2$ center; at 296 K a broad, featureless resonance was observed at $g_{iso} = 2.02$.

The UV−vis spectrum (Figure 16) of $(smif)_2Mn$ features the "red IL band" at 588 nm with the largest molar absorptivity

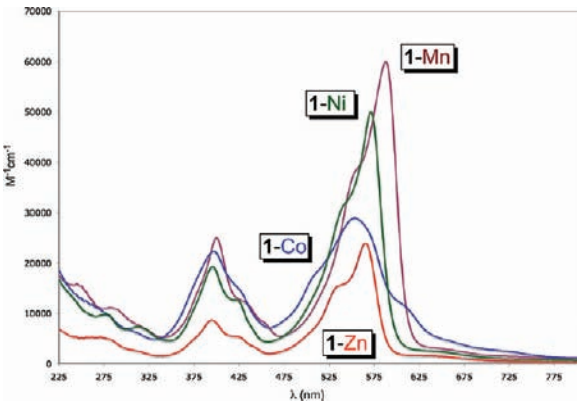

Figure 16. UV−vis spectra of $[(smif)_2M]$ (**1**-M; M = Mn, Co, Ni, Zn) in pentane.

observed ($\varepsilon \approx 60\,000$ M^{-1} cm^{-1}), a shoulder at 557 nm ($\varepsilon \approx 39\,000$ M^{-1} cm^{-1}) that is either a vibrational component or another IL band, and a single "blue IL band" at 400 nm ($\varepsilon \approx 25\,000$ M^{-1} cm^{-1}). Lower energy shoulders off the latter band at 442 ($\varepsilon \approx 13\,000$ M^{-1} cm^{-1}) and 457 ($\varepsilon \approx 8000$ M^{-1} cm^{-1}) are likely to be additional IL absorptions or charge-transfer bands. Note that the situation has reversed from Figure 12; now the lower energy IL band is the most intense, and it is blue-shifted from where the $\nu_{GS} = 0$ to $\nu_{ES} = 0$ components were proposed for **1**-Cr and **1**-Fe. There are also smaller features at ∼635 and ∼750 nm that are common to **1**-M where M = Zn, Co, and Ni. These are likely to be triplet absorptions affiliated with the IL transitions with significant singlet character admixed.

The UV−vis features of **1**-Mn are remarkably similar to the broader IL absorptions of $[(smif)_2Mn]OTf$ (**1**$^+$-Mn, Figure 14), which are observed at 570 ($\varepsilon \approx 26\,000$ M^{-1} cm^{-1}) and 399 nm

dx.doi.org/10.1021/ic200376f | Inorg. Chem. 2011, 50, 12414−12436

($\varepsilon \approx 9{,}700\ M^{-1}cm^{-1}$). While no X-ray crystal structure of $\mathbf{1}^{+}$-Mn was obtained, SQUID magnetometry revealed a μ_{eff} of 5.43 for the cation (Figure 11) augmented by a slight amount of TIP, but with a noticeably greater amount of ZFS. In D_{2d} symmetry, the d_{z^2} (a_1) and $d_{x^2-y^2}$ (b_1) orbitals are intrinsically different, hence a significant ZFS is expected for a high spin d^4 configuration. In addition, the μ_{eff} value is high for an $S = 2$ center (μ(spin only) = 4.9 μ_B) that should have no orbital contribution. A Guoy balance measurement afforded a μ_{eff} of 5.0 μ_B, which is certainly closer to the spin-only moment, yet still high. Spin−orbit contributions from triplet states with significant orbital angular momentum can be the origin of upward deviations from the spin-only value for Mn(III).

5. Cobalt. Two molecules of $(smif)_2Co$ (**1**-Co) were again present in the asymmetric unit, but in this case the metric parameters of the two were statistically distinct. In molecule one, two significantly different $d(CoN_{aza})$ of 1.946(3) and 1.888(3) Å are accompanied by two $d(CoN_{py})$ sets that average 2.184(13) Å and 1.971(13) Å, respectively. The resulting C_{2v} distortion is augmented by a C_s distortion evident in the $N_{aza}CoN'_{aza}$ angle of 177.30(11)° and N_{aza}−Co−N'_{py} angles that vary from 95 to 101°. Molecule two has roughly identical CoN_{aza} distances of 1.945(3) and 1.939(3) Å with accompanying CoN_{py} average distances of 2.105(16) and 2.053(5) Å, respectively. While the remaining core angles are similar to molecule one, its distortion is best construed as C_2.

In stark contrast to the structural vagaries of $(smif)_2Co$ (**1**-Co), the corresponding diamagnetic cation $[(smif)_2Co]OTf$ ($\mathbf{1}^{+}$-Co) has a regular D_{2d} structure with shorter bond distances attributable to low spin Co(III): $d(CoN_{aza})$ = 1.8768(11) Å and $d(CoN_{py})$ = 1.9252(19) Å. The $N_{aza}CoN'_{aza}$ angle approaches linearity at 179.05(10)°, and the average $N'_{aza}CoN'_{py}$ and $N_{py}CoN'_{py}$ angles of 96.1(7)° and 90.7(19)°, respectively, are a testament to the regularity of the structure.

The μ_{eff} of 2.8 μ_B obtained for $(smif)_2Co$ (**1**-Co) by Evans' measurements (6 trials) at 293 K was confirmed by Gouy balance (2.8 μ_B at 294 K), prompting further investigation. As implied by the room temperature measurements, spin crossover behavior was observed in SQUID magnetometry data, as revealed by a decline in the μ_{eff} from 3.19 μ_B at 300 K to 1.75 μ_B at 10 K.[85] The Evans'[71] and Gouy balance values are consistent with a rough 1:1 mixture of S = 3/2 and S = 1/2 species at room temperature; at temperatures <100 K, there is little high spin Co(II) remaining.

Figure 17 illustrates the EPR spectrum of $(smif)_2Co$ (**1**-Co) at 30 K, where virtually all of the Co is in the S = 1/2 configuration. The temperatures at which the S = 3/2 species has a reasonable concentration typically lead to broadened signals due to increased relaxation and they are often not observed; no signals were observed in toluene solution at 296 K. While S = 1/2 species can be often seen at room temperature, in this instance exchange with the S = 3/2 species may be rapid, and other relaxation mechanisms are also common. The cobalt hyperfine couplings in this rhombic system are quite uniform, ranging from 48 to 66 G (140−200 MHz), and differ from related coordination compounds such as $[(terpy)_2Co]^{2+}$ (Co hyperfine) in which the coupling is disparate.[85]

Despite the spectroscopic investigations, the origin of the structural discrepancy between the two molecules in the asymmetric unit is still uncertain, and there were different scenarios that could explain the data. The crystal structure reported above was obtained at 100 K using the Cornell High Energy Synchrotron Source (CHESS), but a second set was also obtained at 173 K on a conventional diffractometer. While the data in the latter collection resulted in a lesser quality solution, the metric parameters for the two essentially matched, and the two molecules in the asymmetric unit were still statistically different. Neither molecule could be attributed to an S = 3/2 species, as both sets of bond distances were more consistent with a low spin Co species, and calculated high spin versions gave metric parameters that were well off the experimental values.

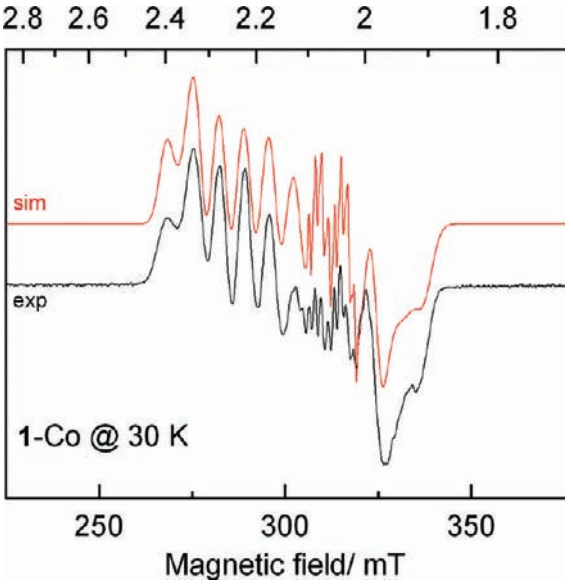

Figure 17. EPR spectrum ($d\chi''/dB$) of rhombic S = 1/2 $(smif)_2Co$ (**1**-Co, I = 7/2) and fit (red): g_x = 2.01, A_x(Co) = 140 MHz (4.67 × 10^{-3} cm^{-1}); g_y = 2.14, A_y(Co) = 200 MHz (6.67 × 10^{-3} cm^{-1}); g_z = 2.21, A_z(Co) = 200 MHz (6.67 × 10^{-3} cm^{-1}). The fit includes a 0.1% impurity modeled as an isotropic species with g = 2.055, A(Co) = 50 MHz (1.67 × 10^{-3} cm^{-1}), and a line width 1/7 of the others.

While it is conceivable that "crystal packing" effects determine the different geometries in the asymmetric unit, it seems very unlikely that such modest interactions can change bond distances to the degree that is observed. Furthermore, inspection of the asymmetric unit failed to uncover a significant interatomic interaction capable of inducing a significant structural change. The remaining scenario regarding the independent geometries is the possibility of several S = 1/2 ground states of nearly the same energy. Although this has been probed and verified by high-level calculations,[63] one additional experiment was conducted to limit the scope of plausible S = 1/2 states, since initial calculations suggested an electronic configuration of $(d_{xy})^2(d_{xz},d_{yz})^4(CNC^{nb})^4(smif\text{-}\pi^*)^1$ (Figure 4), that is, a low-spin Co(III) center and an additional electron in a π^* orbital of the smif ligand.

Metal K-edge X-ray absorption spectroscopic measurements[82−84] were utilized to assign the orbital parentage of the odd electron in S = 1/2 $(smif)_2Co$ (**1**-Co) through comparison to $[(smif)_2Co]OTf$ ($\mathbf{1}^{+}$-Co). As Figure 18 illustrates, a significant shift (~2 eV) in the leading edge to higher energies is observed when **1**-Co is oxidized to $\mathbf{1}^{+}$-Co. In addition, the 1s to 3d pre-edge features are also shifted by ~1.5 eV, consistent with a metal-based, rather than ligand-based, oxidation process. The data clearly portray the electronic configuration from Figure 4 as incorrect, and **1**-Co is thus considered a Co(II) complex. As a consequence, the two distinct geometries evident in the crystal

dx.doi.org/10.1021/ic200376f | Inorg. Chem. 2011, 50, 12414−12436

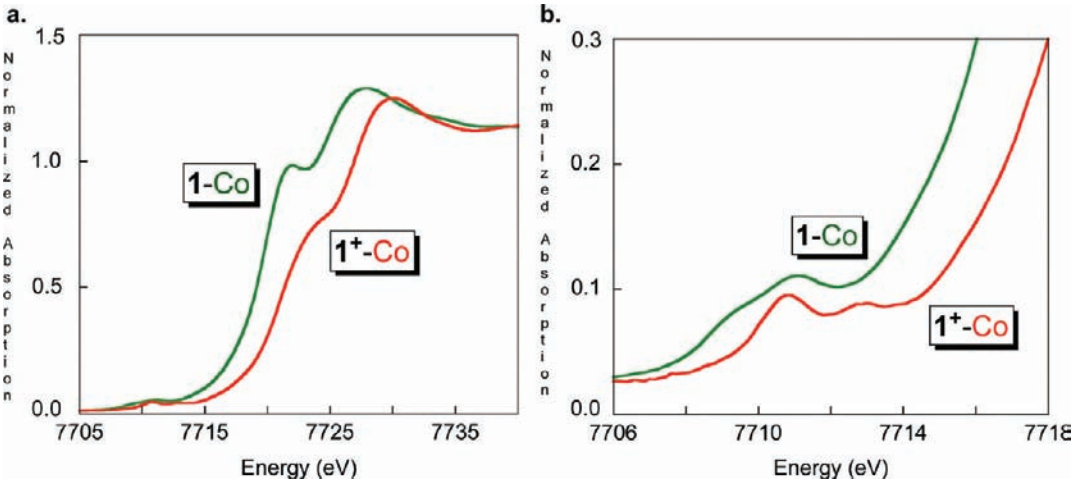

Figure 18. (a) Comparison of the Co K-edge spectra (10 K) for $(smif)_2Co$ (**1**-Co) and $[(smif)_2Co]OTf$ (**1**$^+$-Co) that indicates an increase of ~2 eV in the effective nuclear charge on Co upon oxidation. (b) Expansion of the pre-edge region, showing that the ligand field has increased by ~1.5 eV upon oxidation.

structure of **1**-Co are likely to be two $S = 1/2$ Co(II) species whose energies are close.

If the conventional electronic assessment of $(smif)_2Co$ (**1**-Co) as Co(II) is correct, its UV−vis spectrum should be significantly different than that of the corresponding cation, $[(smif)_2Co]OTf$ (**1**$^+$-Co). From views of Figures 14 and 16, this is correct, although each spectrum is dominated by the IL features common to all *bis*-smif derivatives. The "red IL" absorption in **1**-Co has a maximum at 555 nm ($\varepsilon \approx 29\,000$ M^{-1} cm^{-1}) with a low energy shoulder at ~610 nm and a high energy shoulder at ~515 nm that may be construed as vibrational components. Very low energy features at ~666 nm and ~724 nm are likely to be triplet states that accompany the intense IL transitions. There are additional complications due to the possibility of LMCT bands, and the band shape of the 555 nm absorption is distorted enough to encourage speculation. A single "blue IL" band is observed at 400 nm ($\varepsilon \approx 22\,100$ M^{-1} cm^{-1}) and it has shoulders consistent with additional IL or CT absorptions. The cation **1**$^+$-Co has a broad, featureless band at 591 nm ($\varepsilon \approx 23\,000$ M^{-1} cm^{-1}) assigned to the "red IL" band, and two less intense "blue IL" absorptions at 385 ($\varepsilon \approx 13\,000$ M^{-1} cm^{-1}) and 320 nm ($\varepsilon \approx 12\,000$ M^{-1} cm^{-1}) with a low energy shoulder on the former.

6. Nickel. In $(smif)_2Ni$ (**1**-Ni), the $d(NiN_{aza})$ and $d(NiN_{py})$ distances of 2.019(5) and 2.093(9) Å are elongated relative to Co because of the single occupation of two sigma-antibonding orbitals, according to Figure 4. Only high spin d^5 $(smif)_2Mn$ (**1**-Mn) has longer distances among the first row metals whose covalent radii are roughly the same. The remaining parameters reveal subtle C_2 and C_s distortions to the two molecules in the asymmetric unit.

$(smif)_2Ni$ (**1**-Ni) is "EPR silent", indicative of a ZFS large enough to obviate X-band observation. SQUID magnetometry (Figure 11) indicates a μ_{eff} of 2.81 μ_B at 300 K and a modest decline below 10 K because of ZFS. The UV−vis spectrum of **1**-Ni consists of dominant "red IL" band at 571 ($\varepsilon \approx 50\,000$ M^{-1} cm^{-1}) with a shoulder at ~540 nm ($\varepsilon \approx 31\,500$ M^{-1} cm^{-1}), and a lesser "blue IL" absorption at 398 nm ($\varepsilon \approx 19\,000$ M^{-1} cm^{-1}) with a low energy shoulder at ~425 nm ($\varepsilon \approx 12\,000$ M^{-1} cm^{-1}). A low-lying absorption at 652 nm ($\varepsilon \approx 2300$ M^{-1} cm^{-1}) is consistent with triplet excitation affiliated with an IL band, as has been observed in several previous cases. All spectral measurements are consistent with a standard d^8 Ni(II) center.

7. Zinc. $(smif)_2Zn$ (**1**-Zn) was prepared by Westerhausen[25] and structurally characterized, thus the examination of diamagnetic **1**-Zn was limited to standard NMR characterization and UV−vis spectroscopy. The "red IL" band at 566 nm in the spectrum of **1**-Zn is again dominant ($\varepsilon \approx 24\,000$ M^{-1} cm^{-1}), and possesses a high energy shoulder at 537 nm. The single "blue IL" band is at 396 nm ($\varepsilon \approx 8700$ M^{-1} cm^{-1}) with a series of low energy shoulders consistent with a vibrational progression of ~1200 cm^{-1} similar to those previously observed. The low-lying absorption at ~635 nm may be attributed to a triplet corresponding to an IL band.

8. Ruthenium, Rhodium, and Iridium. The two second row complexes, $(smif)_2Ru$ (**1**-Ru) and $[(smif)_2Rh]OTf$ (**1**$^+$-Rh), and the third row $[(smif)_2Ir]BPh_4$ (**1**$^+$-Ir) are all low spin, diamagnetic d^6 derivatives that were not structurally characterized. Each possesses five ^1H NMR spectral resonances and six $^{13}C\{^1H\}$ NMR signals indicative of D_{2d} symmetry in solution, and the usual intense UV−vis spectral bands associated with the smif IL transitions (Figure 19). The

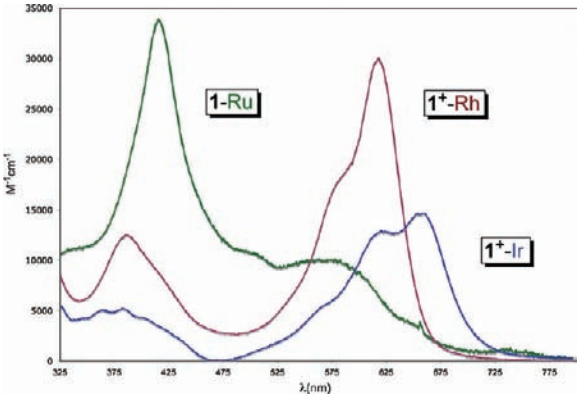

Figure 19. UV−vis spectra of $(smif)_2Ru$ (**1**-Ru), $[(smif)_2Rh]OTf$ (**1**$^+$-Rh), and $[(smif)_2Ir]BPh_4$ (**1**$^+$-Ir).

spectrum of **1**-Ru reveals the "red IL band" at 566 nm ($\varepsilon \approx 10\,000$ M^{-1} cm^{-1}) as a broad featureless absorbance flanked by a lesser shoulder at ~650 nm ($\varepsilon \approx 3600$ M^{-1} cm^{-1}) and a band at 740 nm

dx.doi.org/10.1021/ic200376f | Inorg. Chem. 2011, 50, 12414–12436

($\varepsilon \approx 1000\ M^{-1}\ cm^{-1}$). The latter two absorptions may be triplets affiliated the IL transitions, most likely the intense "blue IL" transition at 417 nm ($\varepsilon \approx 33\,000\ M^{-1}\ cm^{-1}$). A band at ~505 nm ($\varepsilon \approx 10\,500\ M^{-1}cm^{-1}$) is likely to be another IL component or an MLCT transition.

The lowest energy IL bands, that is, the "red-IL bands", are red-shifted in $[(smif)_2Rh]OTf$ ($\mathbf{1}^+$-Rh), and $[(smif)_2Ir]BPh_4$ ($\mathbf{1}^+$-Ir) relative to $(smif)_2Ru$ (**1**-Ru), and they are the most intense, a change also seen when $(smif)_2Fe$ (**1**-Fe) is compared to $(smif)_2Co$ (**1**-Co) and $[(smif)_2Co]OTf$ ($\mathbf{1}^+$-Co). For $\mathbf{1}^+$-Rh, the 618 nm ($\varepsilon \approx 30\,000\ M^{-1}\ cm^{-1}$) absorption has a shoulder at 580 nm ($\varepsilon \approx 17\,600\ M^{-1}\ cm^{-1}$), and these are significantly more intense than the "blue IL band" at 385 nm ($\varepsilon \approx 12\,400\ M^{-1}\ cm^{-1}$) with its accompanying shoulder at 425 nm ($\varepsilon \approx 7300\ M^{-1}\ cm^{-1}$). The typical IL features are attenuated in $\mathbf{1}^+$-Ir, whose most prominent absorption occurs at 658 nm ($\varepsilon \approx 14\,700\ M^{-1}\ cm^{-1}$), with apparent vibrational components at 623 nm ($\varepsilon \approx 12\,900\ M^{-1}\ cm^{-1}$) and 570 nm ($\varepsilon \approx 5800\ M^{-1}\ cm^{-1}$). Its "blue IL band" has an apparent vibrational progression witnessed as similarly intense ($\varepsilon \approx 5000\ M^{-1}\ cm^{-1}$) absorptions at 405, 386, 366, and 346 nm.

DISCUSSION

Syntheses of $(smif)_2M$ and $(smif)_2M^+$. An unusual series of neutral "Werner complexes" has been prepared by using the 1,3-di-(2-pyridyl)-2-azaallyl ligand, coined "smif". Straightforward metatheses of transition metal salts with (smif)M (M = Li, Na), and the addition of 1,3-di-(2-pyridyl)-2-azapropene, (smif)H, to appropriate metal amides led to the desired $(smif)_2M$ (**1**-M, M = Cr, Mn, Fe, Co, Ni, Ru) and $[(smif)_2Ir]BPh_4$ ($\mathbf{1}^+$-Ir) complexes in modest to excellent yields. An additional reducing equiv was used to prepare $(smif)_2V$ (**1**-V) from $VCl_3(THF)_3$, and, surprisingly, the oxidant AgOTf was compatible with the smif anion during the course of its reaction with $Rh_2(O_2CCF_3)_4$ to afford $[(smif)_2Rh]OTf$ ($\mathbf{1}^+$-Rh). Presumably this is a fortunate circumstance of relative reagent solubilities and relative rates. Using electrochemical measurements as a guide, mild Ag^+ oxidations cleanly provided $[(smif)_2M]OTf$ ($\mathbf{1}^+$-M; M = Cr, Mn, Co). For those oxidations that failed despite favorable electrochemical indications, it is likely that reactions of the CNC-backbone of the smif ligand,[48,57] perhaps due to ligand-based oxidations,[86] lead to degradation of cations on a chemical time scale that is slower than the sweep rates used in the CV experiments.

Electronic Factors Influencing $(smif)_2M$ and $(smif)_2M^+$ Structures. A number of the $(smif)_2M$ (**1**-M, M = V, Cr, Mn, Fe, Co, Ni) and $[(smif)_2M]OTf$ ($\mathbf{1}^+$-M; M = Cr, Co) complexes have been structurally characterized and details have been given above. In general, deviations from D_{2d} symmetry may be construed as arising from their d-counts and the <180° bite angle ($N_{py}-M-N_{py}'$) intrinsic to the smif ligand. As compared to rigorously octahedral species, the electronic asymmetry inherent to 6-coordinate D_{2d} complexes manifests itself in EPR spectra and SQUID measurements, but these contributions are minor.

The most symmetric species are the low spin d^6 complexes $[(smif)_2Co]OTf$ ($\mathbf{1}^+$-Co) and $(smif)_2Fe$ (**1**-Fe), and the d^3 chromium cation, $[(smif)_2Cr]OTf$ ($\mathbf{1}^+$-Cr), which all have short $d(M-N_{aza})$ and $d(M-N_{py})$ consistent with significant ligand field stabilization energies. The most distorted of the remaining cases is $(smif)_2Mn$ (**1**-Mn). Its high spin d^5 configuration leads to long metal–ligand distances and weaker bonding, and the expected lack of covalency for Mn(II) renders the coordination sphere highly susceptible to the minor structural perturbations. There is no indication from the SQUID and EPR data that the molecule has significant distortions due to electronic factors. The *bis*-smif nickel derivative, **1**-Ni, also has only small distortions, consistent with its $^3B_2$ ground state (i.e., $(d_{z^2})^1(d_{x^2-y^2})^1$), and the core distances are long, as expected for pseudo-octahedral Ni(II).

The cobalt derivative $(smif)_2Co$ (**1**-Co), whose structure at 100 K represents a low spin d^7 configuration according to K-edge spectroscopy, is considerably distorted from D_{2d} symmetry in each statistically different, independent molecule. In principle, the $^2B_2$ state (D_{2d}) should reflect an axial compression/equatorial elongation, and vice versa for a $^2A_1$ state, but such standard distortions are not compatible with tridentate ligands. One molecule of **1**-Co shows a clear asymmetry (C_{2v}) in the binding of the two smif ligands, with one roughly 0.06 Å closer to the cobalt at the N_{aza} position and 0.21 Å closer at the pyridine-N positions. The distortion of the second molecule is not so clearly seen, but a C_2 twist is the main change.

The most interesting GS configurations belong to the vanadium and chromium derivatives, $(smif)_2V$ (**1**-V) and $(smif)_2Cr$ (**1**-Cr), respectively. A C_s distortion is found for **1**-V, and the $N_{aza}-V-N_{aza}'$ angle of 172.1(4)° is the most severe cant of a smif seen aside from those found for **1**-Mn. If the compound was a true D_{2d} d^3 V(II) system (i.e., $^4B_1$), no orbital impetus for such a distortion would be expected. The EPR spectrum (Figure 10) also reveals a modest but significant distortion in the $S = 3/2$ system, and SQUID magnetometry (Figure 11) indicates a large ZFS not expected for a d^3 configuration (cf $[(smif)_2Cr]OTf$ ($\mathbf{1}^+$-Cr)). The "d_{yz} orbital" in the calculation of **1**-V is the HOMO in the system, and its composition is greatly mixed with a ligand π^* component. It is possible the system should be considered (smif(−))-(smif(2−))V(III), that is, the smif ligand is redox noninnocent, but this would require a *ferromagnetic coupling* of the smif electron with the remaining d^2 core, whereas the opposite is seen for **1**-Cr. When an electron is promoted into a ligand, the spatial separation from the remaining valence electrons causes a decrease in coulomb or exchange energy affiliated with every pairwise exchange. For a pseudo-octahedral d^3 case, "redox noninnocence" would actually cause a loss in exchange energy (stabilization) that would need to be compensated by the stability of the $d^2\pi^{*1}$ configuration. If the calculations in Figure 3 are reasonable, the smif π^* orbitals are still energetically far from the "t_{2g}" set, and it may not be feasible for the transfer to occur. Instead the HOMO is highly mixed, and the compound behaves as a standard $S = 3/2$ system, albeit with the modest asymmetry indicated by a large ZFS, which may be derived from the a significant ligand component to the GS configuration. Unfortunately, K-edge measurements, which could provide greater insight into the GS composition, were not obtained on **1**-V. The distances of the core are consistent with either V(II) or V(III) since the electron in question with either occupy a π^b d-orbital or a ligand π^*-orbital and the latter would not be expected to impart a noticeable bond length change from the former.

In the case of $(smif)_2Cr$ (**1**-Cr), K-edge spectroscopy suggests that its GS configuration is (smif(−))(smif(2−))Cr-(III), or d^3 Cr(III) *antiferromagnetically coupled* to a smif π^* electron, that is, $d^3\pi^{*1}$. Here it is important to recognize that there are three configurations of interest: high- and low-spin d^4 and $d^3\pi^{*1}$. It is plausible that the high and low spin forms of Cr(II) are likely to be energetically similar, given the above

dx.doi.org/10.1021/ic200376f | Inorg. Chem. 2011, 50, 12414–12436

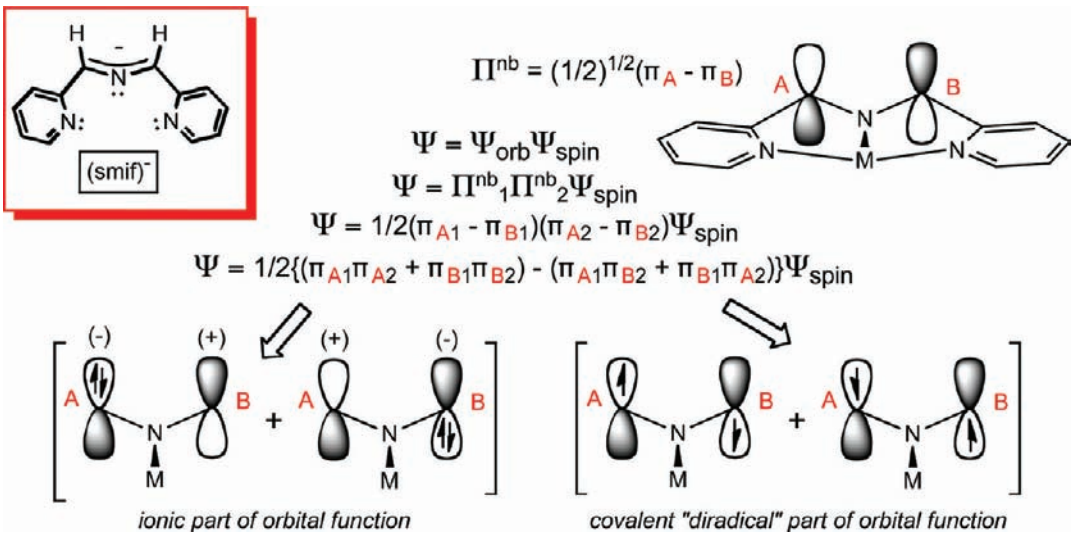

Figure 20. Simplified decomposition of the CNC^{nb} smif backbone "allyl" orbital (p orbital components A and B; electrons 1 and 2), ignoring contributions from pyridine π-orbitals.

assessments of the smif field strength. The resulting redox noninnocent $d^3\pi^{*1}$ configuration represents a situation that relieves the sigma-antibonding character of a HS (high spin) d^4 GS, or one that relieves the coulomb interaction of a LS d^4 GS by spatially separating the "paired electrons". In addition, the pairwise exchange energies in the d^3 core of the Cr(III) center will be more favorable as the 3d orbitals contract. Evidence for the contraction is seen in the d(Cr−N), which compares favorably with those of $[(smif)_2Cr]OTf$ (**1**$^+$-Cr). The difference between the d(Cr−N) of $(bipy)_3Cr^{2+}$ and $(bipy)_3Cr^{3+}$ is about 0.10 Å,[3,87] and it is possible that the former is actually $(bipy)_2(bipy(-))Cr^{3+}$ by the same reasoning. Consistent with this argument is the $\sim 10^9$ M^{-1} s^{-1} self-exchange rate for $(bipy)_3Cr^{2+/3+}$, which is only sensible if the chromous center is low spin or contains a redox "noninnocent" bipy ligand.[88]

The EPR spectrum of $(smif)_2Cr$ (**1**-Cr) is shown in Figure 13 and simulated as a "very low |D|", $S = 1$ system. It is unusual to find observable $S = 1$ systems, and this particular case may be justified by rationalizing the chromium to be a highly symmetric Cr(III) center AF-coupled to a smif radical dianion. It is conceivable that in related Cr(II) systems with potentially redox active ligands, *EPR spectra may provide a signature for redox active ligands antiferromagnetically coupled to metals.* Fast electron transfer rates, such as the self-exchange rates, may also be indicative of electrons in redox "noninnocent" ligands.

UV−vis Spectroscopy. The individual descriptions of the $(smif)_2M^{0/+}$ species are familiar in the sense that most of their spectroscopic and magnetic behavior typifies Werner-type coordination compounds, with modest changes intrinsic to the *bis*-smif framework. The individual species have already been discussed above.

The major difference in *bis*-smif derivatives, relative to simpler N-donor complexes, stems from the unique electronic features of the smif anion, and its HOMO, the CNC^{nb} backbone orbital with opposing phases on the carbons adjacent to the nitrogen that contains a nodal plane (Figure 20). Transitions arising from the promotion of electrons in these orbitals (Figure 3; linear combinations a_2 and b_1) to smif π^* orbitals located mostly on the pyridines are the origin of the "red IL" and "blue IL" UV−vis bands in each *bis*-smif compound. The HOMOs of $[(smif)_2M]^n$ ($n = 0$, **1**-M; $n = 1$, **1**$^+$-M) have considerable anionic character localized on the CNC^{nb} portion of the orbitals, and transfer of this charge to the pyridines in the IL excited states renders a large change in dipole moment. The resulting intensities of the IL bands dwarf those of the MLCT bands common to virtually all other Werner complexes.[3−40] Betley's recent examination of dipyrromethane and related ligands[89,90] revealed extraordinary UV−vis absorption intensities due to related intraligand transitions, and it appears that smif shares some of their features. Figure 20 illlustrates a simple view of the CNC^{nb} orbital, where its carbon backbone p-orbital components can be shown to possess either ionic or covalent "diradical" character, according to the expansion of the orbital component of its wave function. In a future submission, the C−C bond-forming chemistry originating from the CNC^{nb} backbone will be elucidated.[57]

Because of the nonbonding character of the CNC^{nb} smif orbitals (Figure 3), they are energetically near the d-orbitals for all the first row metals. For $(smif)_2M$ (**1**-M, M = V, Cr, and likely Mn), they are slightly below the "t_{2g}" set, for **1**-Fe they are slightly above the "t_{2g}" orbitals, and for **1**-M (M = Co, Ni), they are amid the pseudo-octahedral field. For all **1**-M calculated, the CNC^{nb} orbitals are not substantially perturbed by changes in M, nor are the corresponding smif π^*-orbitals, hence the relative consistency of the "red IL" ($\lambda_{max} \approx 590(30)$ nm and "blue IL" ($\lambda_{max} \approx 420(40)$) band maxima. Unfortunately, the intensity of these bands obscures much of the other features of interest, and makes locating d-d bands implausible.

The tremendous intensities of the IL bands permit ready identification in all of the UV−vis spectra pertaining to $(smif)_2M$ (**1**-M) aside from **1**-V, and the "red IL" bands often feature an apparent vibrational progression, typically around $\sim 1100-1200$ cm^{-1}.[43] IR spectra of **1**-M manifest several absorptions in this region, and it is likely that the relevant excited states feature similar vibrations that are appropriately coupled. In some instances, similar progressions are observed for the "blue IL" transitions, although the vibrations appear at slightly higher frequencies. There is a noticeable change in the relative intensities of the IL bands upon moving from **1**-Zn to **1**-V. For **1**-Zn to **1**-Co, the "red IL" band is significantly more intense than its blue partner, whereas for **1**-Fe, $(o$-Mesmif$)_2$Fe

dx.doi.org/10.1021/ic200376f | *Inorg. Chem.* 2011, 50, 12414−12436

(**2**-Fe), and **1**-Cr, the situation subtly reverses. The breadth of these absorptions, whether due to vibrational progressions or multiple IL transitions, hampers the determination of the overall relative intensities. Interestingly, the high spin **1**-Mn and (o-Me$_2$smif)$_2$Fe (**3**-Fe) cases clearly have "red IL" bands that are significantly more intense than their "blue IL" counterparts. In the cations [(smif)$_2$M]$^+$ (**1**$^+$-M, M = Cr, Mn, Co, Rh, Ir), the "red IL" band is clearly dominant, even for the second row species, yet the neutral **1**-Ru has a similar overall spectrum as its iron congener.

The majority of the complexes exhibit weaker features between 650 and 1100 nm (the spectra are devoid of absorptions to 1700 nm). These are formulated as singlet → triplet absorptions whose intensity may be dependent on how well the metal helps the "intensity stealing", that is, how effective the metal aids in mixing singlet character into the triplet wave functions of the excited states. Calculations on the lowest lying triplet state of (smif)$^-$ place it ∼1.3 eV above the singlet. Using this as a guide,[91] the weak features are likely to be triplet components of the "blue IL" bands, since they lie ∼1.0−1.7 eV below the 380−440 nm region.

The similarity of the IL and plausible MLCT features in UV−vis spectra of (smif)$_2$Cr (**1**-Cr) and [(smif)$_2$Cr]OTf (**1**$^+$-Cr) provided a corroboration of the proposed electronic configuration of **1**-Cr as (smif(−))(smif(2−))Cr(III), the redox noninnocence of smif. However, the spectrum of **1**-Cr shows features too intense to be S → T absorptions in the region from 675−850 nm ($\varepsilon \approx 6{,}000$ M^{-1} cm^{-1}). The existence of a redox "noninnocent" ligand containing an electron in a π^*-orbital is often detected via the appearance of an intervalence charge transfer (IVCT) band,[72−76] which can be vibrationally broadened.[74] A low energy, that is, in the red or near IR, IVCT band is featured in systems having one normal ligand and one possessing radical character, and is often very intense, with extinction coefficients as high as 60 000 M^{-1} cm^{-1}. In many of these cases, the π-systems responsible for the transition are roughly coplanar, as in square planar complexes. In (smif)$_2$Cr, the π-systems of the smif ligands are essentially orthogonal. If these bands are of the IVCT type and not MLCT transitions, perhaps the orthogonality of the smif π^*-orbitals are attenuating the intensities.

■ CONCLUSIONS

In contrast to typical cationic coordination compounds, neutral, hydrocarbon soluble, "Werner complexes" [(smif)$_2$M]^n (n = 0, **1**-M, M = V, Cr, Mn, Fe, Co, Ni, Zn, Ru; n = 1, **1**$^+$-M, M = Cr, Mn, Co, Rh, Ir; smif =1,3-di-(2-pyridyl)-2-azaallyl) and the related azaallyl species (^{o}Mesmif)$_2$Fe (**2**-Fe) and (^{o}Me$_2$smif)$_2$Fe (**3**-Fe) have been prepared. While similar in field strength to terpy and other tridentate N-donors, the smif complexes are distinguished by extremely intense intraligand aborptions in blue and red regions of UV−vis spectrum. In one instance, the smif ligand has been shown to be redox "noninnocent", and the singlet diradical character of the ligand HOMO suggests potential reactivity at the ligand CNC-backbone.[48,49,57]

■ EXPERIMENTAL SECTION

General Considerations. All manipulations were performed using either glovebox or high vacuum line techniques. All glassware was oven-dried. THF and ether were distilled under nitrogen from purple sodium benzophenone ketyl and vacuum transferred from the same prior to use. Hydrocarbon solvents were treated in the same manner with the addition of 1−2 mL/L tetraglyme. Benzene-d_6 and toluene-d_8 were dried over sodium, vacuum transferred and stored over activated 4 Å molecular sieves. THF-d_8 was dried over sodium and vacuum transferred from sodium benzophenone ketyl prior to use. $VCl_3(THF)_3$,[58] $CrCl_2(THF)$,[41] $Cr\{N(TMS)_2\}(THF)_2$,[42] $FeBr_2(THF)_2$,[53] $Fe\{N(TMS)_2\}_2(THF)$,[52] $NiCl_2(DME)$,[54] sodium bis(trimethylsilyl)amide,[51] and 1,3-di-(2-pyridyl)-2-azapropene (smifH)[50] were prepared according to literature procedures. Lithium bis(trimethylsilyl)amide was purchased from Aldrich and recrystallized from hexanes prior to use. All other chemicals were commercially available and used as received.

NMR spectra were obtained using an INOVA 400 and 500 MHz spectrometers. Chemical shifts are reported relative to benzene-d_6 (^{1}H δ 7.16; ^{13}C{^{1}H} δ 128.39), toluene-d_8 (^{1}H δ 2.09; ^{13}C{^{1}H} δ 20.4), and THF-d_8 (^{1}H δ 3.58; ^{13}C{^{1}H} δ 67.57). Infrared spectra were recorded on a Nicolet Avatar 370 DTGX spectrophotometer interfaced to an IBM PC (OMNIC software). UV−vis spectra were obtained on a Shimadzu UV-2102 interfaced to an IBM PC (UV Probe software). Solution magnetic measurements were conducted via Evans' method in toluene-d_8.[71] Solid state magnetic measurements were performed using a Johnson Matthey magnetic susceptibility balance calibrated with $HgCo(SCN)_4$. Elemental analyses were performed at the University of Erlangen-Nuremberg and Robertson Analytical (New Jersey).

Procedures. *1. °MesmifH.* To a suspension of anhydrous $MgSO_4$ (12.421 g, 103.19 mmol) in 40 mL of CH_2Cl_2 was added 6-methyl-2-pyridinecarboxaldehyde (2.500 g, 20.64 mmol) followed by the slow addition of 2-(aminomethyl)pyridine (2.232 g, 20.64 mmol). The suspension stirred at 23 °C for 3 h. The reaction mixture was filtered and washed with CH_2Cl_2. The solvent was removed under vacuum to yield a pale yellow liquid (4.25 g, 97%). ^{1}H NMR (C_6D_6, 400 MHz): δ 2.39 (s, CH_3, 3 H), 4.92 (s, CH_2, 2 H), 6.60 (d, py^{Me}-C^5H, 1 H, J = 7.6 Hz), 6.61 (t, py-C^5H, 1 H, J = 5.3 Hz), 7.04 (t, py^{Me}-C^4H, 1 H, J = 7.6 Hz), 7.08 (td, py-C^4H, 1 H, J = 7.5, 1.6 Hz), 7.20 (d, py-C^3H, 1 H, J = 7.8 Hz), 8.02 (d, py^{Me}-C^3H, 1 H, J = 7.8 Hz), 8.48 (d, py-C^6H, 1 H, J = 4.8 Hz), 8.61 (s, im-CH, 1 H). ^{13}C{^{1}H} NMR (C_6D_6, 100 MHz): δ 24.62 (CH_3), 67.24 (CH_2), 118.48 (py^{im}-C^{3}H), 122.16 (py-C^{3}H), 122.53 (py^{im}-C^{5}H), 124.39 (py-C^{5}H), 136.36 (py-C^{4}H), 137.70 (py^{im}-C^{4}H), 149.95 (py-C^{6}H), 154.25 (py^{im}-C^6), 158.54 (py^{im}-C^2), 160.22 (py-C^2), 164.97 (im-CH).

2. °Me$_2$smifH. To a suspension of anhydrous $MgSO_4$ (5.036 g, 41.82 mmol) in 16 mL of CH_2Cl_2 was added 6-methyl-2-pyridinecarboxaldehyde (1.014 g, 8.37 mmol) followed by the slow addition of 6-methyl-2-pyridylmethylamine (1.022 g, 8.37 mmol). The yellow suspension stirred at 23 °C for 3 h. The reaction mixture was filtered and washed with CH_2Cl_2. The solvent was removed under vacuum to yield a pale yellow solid (1.73 g, 92%). ^{1}H NMR (C_6D_6, 500 MHz): δ 2.38 (s, py-CH_3, 3 H), 2.39 (s, py^{im}-CH_3, 3 H), 4.93 (s, CH_2, 2 H), 6.61 (d, py-C^3H, py-C^4H, 2 H, J = 6.5 Hz), 7.06 (t, py^{im}-C^4H, 1 H, J = 7.5 Hz), 7.10 (d, py-C^5H, py^{im}-C^5H, 2 H, J = 7 Hz), 8.02 (d, py^{im}-C^3H, 1 H, J = 8 Hz), 8.62 (s, CH, 1 H). ^{13}C{^{1}H} NMR (C_6D_6, 125 MHz): δ 24.62 (py-CH_3), 24.84 (py^{im}-CH_3), 67.45 (CH_2), 118.47 (py-C^{3}H), 119.56 (py^{im}-C^{3}H), 121.60 (py-C^{5}H), 124.36 (py^{im}-C^{5}H), 136.70 (py-C^{4}H), 136.78 (py^{im}-C^{4}H), 155.38 (py^{im}-C^2), 158.46 (py-C^6), 158.50 (py^{im}-C^6), 159.46 (py-C^2), 164.79 (im-CH).

3. Li(smif). To a solution of lithium bis(trimethylsilyl)amide (1.273 g, 7.60 mmol) in 50 mL THF was slowly added a solution of smifH (1.500 g, 7.60 mmol) in 50 mL THF at −78 °C under argon. The solution immediately turned magenta and was stirred at −78 °C for 2 h. After the mixture was stirred at 23 °C for 2 h, the volatiles were removed in vacuo. The solid was triturated with Et_2O and filtered. Li(smif) was isolated as a metallic gold solid (1.389 g, 90%). ^{1}H NMR (C_6D_6, 400 MHz): δ 5.98 (t, py-C^5H, 1 H, J = 8 Hz), 6.50 (d, py-C^3H, 1 H, J = 8 Hz), 6.84 (t, py-C^4H, 1 H, J = 8 Hz), 7.16 (s, CH, 1 H), 7.66 (d, py-C^6H, 1 H, J = 4 Hz). ^{13}C{^{1}H} NMR (C_6D_6, 100 MHz): δ 113.20 (CH), 117.95 (py-C^{3}H), 118.65 (py-C^{5}H), 136.18 (py-C^{4}H), 148.90 (py-C^{6}H), 159.44 (py-C^2).

4. Na(smif). To a solution of sodium bis(trimethylsilyl)amide (1.395 g, 7.60 mmol) in 50 mL THF was slowly added a solution of smifH (1.500 g, 7.60 mmol) in 50 mL THF at −78 °C under argon. The solution immediately turned magenta and was stirred at −78 °C

dx.doi.org/10.1021/ic200376f | Inorg. Chem. 2011, 50, 12414−12436

for 2 h. After it was stirred at 23 °C for 2 h, the volatiles were removed in vacuo. The solid was triturated with Et_2O (3 × 15 mL) prior to filtering. Na(smif) was isolated as a metallic gold solid (1.602 g, 96%). ^{1}H NMR (C_6D_6, 400 MHz): δ 6.19 (t, py-C^5*H*, 1 H, *J* = 5.6 Hz), 6.55 (d, py-C^3*H*, 1 H, *J* = 8 Hz), 6.97 (t, py-C^4*H*, 1 H, *J* = 7.2 Hz), 7.04 (s, C*H*, 1 H), 7.72 (d, py-C^6*H*, 1 H, *J* = 4 Hz). ^{13}C{^{1}H} NMR (C_6D_6, 100 MHz): δ 112.19 (*C*H), 115.70 (py-C^{3}H), 119.05 (py-C^{5}H), 135.62 (py-C^{4}H), 149.81 (py-C^{6}H), 160.23 (py-C^2).

*5. (smif)$_2$V (**1**-V).* To a 50 mL 3-neck flask charged with lithium bis(trimethylsilyl)amide (0.170 g, 1.02 mmol) and 0.95% Na/Hg (1.288 g, 0.53 mmol) was vacuum transferred 10 mL THF at −78 °C. A solution of smifH (0.200 g, 1.01 mmol) in THF (8 mL) was slowly added to the flask via a dropping funnel under argon. The solution immediately turned magenta and stirred at −78 °C for 3 h prior to the addition of $VCl_3(THF)_3$ (0.189 g, 0.51 mmol). The reaction mixture, which turned cherry red after slowly warming to 23 °C and stirring for 12 h, was degassed and filtered. The volatiles were removed in vacuo, and the microcrystalline solid was triturated and filtered in Et_2O to yield 0.185 g of **1**-V (81%). EA attempts failed for this extremely air sensitive material. μ_{eff} (SQUID, 300 K) = 3.76 μ_B.

*6. (smif)$_2$Cr (**1**-Cr).* To a solution of $Cr\{N(SiMe_3)_2\}_2(THF)_2$ (0.425 g, 0.82 mmol) in 8 mL of Et_2O was slowly added a solution of smifH (0.325 g, 1.65 mmol) in 10 mL Et_2O at 23 °C. The solution immediately became dark emerald green. The reaction was degassed, warmed to 23 °C, and stirred for 12 h while dark green crystals precipitated from solution. The reaction was concentrated, and the green suspension was filtered to yield 0.288 g of crystalline **1**-Cr (79%). ^{1}H NMR (C_6D_6, 400 MHz): δ −103.60 ($\nu_{1/2} \approx$ 1700 Hz, py-C*H*, 1 H), −22.67 ($\nu_{1/2} \approx$ 1900 Hz, py-C*H*, 1 H), −19.83 ($\nu_{1/2} \approx$ 200 Hz, py-C*H*, 1 H), 19.35 ($\nu_{1/2} \approx$ 130 Hz, C*H*, 1 H), 22.08 ($\nu_{1/2} \approx$ 100 Hz, py-C*H*, 1 H). Anal. Calcd. $H_{20}C_{24}N_6Cr$: C, 64.86; H, 4.54; N, 18.91. Found: C, 63.81; H, 4.21; N, 17.43 (extreme air sensitivity hampered EA). μ_{eff} (SQUID, 300 K) = 2.67 μ_B.

*7. [(smif)$_2$Cr](OTf) (**1**$^+$-Cr).* To a 25 mL round-bottom flask charged with (smif)$_2$Cr (0.300 g, 0.67 mmol) and AgOTf (0.173 g, 0.67 mmol) was vacuum transferred 8 mL Et_2O at −78 °C, and the reaction mixture became green within 5 min. The flask warmed slowly to 23 °C and was stirred for 2 d while a dark green solid precipitated from the pale blue solution. The volatiles were removed in vacuo. Recrystallization of the dark green solid from THF at 80 °C under a blanket of argon for 16 h led to the formation of metallic red crystals of **1**$^+$-Cr (0.309 g, 75%). ^{1}H NMR (C_6D_6, 400 MHz): δ −12.19 ($\nu_{1/2} \approx$ 600 Hz, py-C*H*, 1 H), −3.95 ($\nu_{1/2} \approx$ 600 Hz, py-C*H*, 1 H). μ_{eff} (Gouy balance, 295K) = 3.6 μ_B; μ_{eff} (SQUID, 300 K) = 3.76 μ_B.

*8. (smif)$_2$Mn (**1**-Mn).* To a solution of lithium bis(trimethylsilyl)-amide (0.425 g, 2.54 mmol) in 15 mL THF at −78 °C was added dropwise a solution of smifH (0.500 g, 2.53 mmol) in 10 mL of THF under argon. The solution immediately turned magenta and stirred at −78 °C for 2 h prior to the addition of $MnCl_2$ (0.160 g, 1.27 mmol). The reaction mixture became deep purple after stirring at 23 °C for 36 h. The volatiles were removed in vacuo, and the solid was dissolved and filtered in toluene. Toluene was removed, and the solid was triturated and filtered in Et_2O to isolate metallic gold crystals of **1**-Mn (0.410 g, 72%). ^{1}H NMR (C_6D_6, 400 MHz): δ −13.52 ($\nu_{1/2} \approx$ 1200 Hz, py-C*H*, 1 H), 48.08 ($\nu_{1/2} \approx$ 4100 Hz, py-C*H*, 1 H). Anal. Calcd. $H_{20}C_{24}N_6Mn$: C, 64.43; H, 4.51; N, 18.78. Found: C, 64.21; H, 4.40; N, 18.52. μ_{eff} (SQUID, 300K) = 5.73 μ_B.

*9. [(smif)$_2$Mn](OTf) (**1**$^+$-Mn).* To a 100 mL round-bottom flask charged with (smif)$_2$Mn (**1**-Mn, 0.700 g, 1.56 mmol) and AgOTf (0.402 g, 1.56 mmol) was vacuum transferred 50 mL THF at −78 °C. The dark magenta-purple solution slowly warmed to 23 °C and darkened to a deeper purple. After stirring at 23 °C for 1.5 d, the volatiles were removed in vacuo resulting in a red-bronze metallic solid which was filtered in toluene and THF. Filtrates were concentrated, cooled to 23 °C, and filtered to yield metallic red-bronze microcrystals of **1**$^+$-Mn (0.728 g, 78%). Anal. Calcd $H_{20}C_{25}N_6O_3F_3SMn$: C, 50.34; H, 3.38; N, 16.66; S, 5.38. Found: C, 50.18; H, 5.50; N, 12.75; S, 5.56. μ_{eff} (Gouy balance, 295K) = 4.45 μ_B; μ_{eff} (SQUID, 300 K) = 5.43 μ_B.

*10. (smif)$_2$Fe (**1**-Fe).* **a.** To a solution of $Fe\{N(SiMe_3)_2\}_2(THF)$ (0.284 g, 0.63 mmol) in 15 mL Et_2O was slowly added a solution of smifH (0.250 g, 1.27 mmol) in Et_2O (15 mL) at 23 °C. The solution immediately changed from pale green to deep forest green. The reaction was degassed and warmed to 23 °C. Black-metallic purple crystals began to precipitate from solution after stirring for 30 min. The reaction mixture was stirred for an addition 9.5 h. The volatiles were removed, and the solid was triturated and filtered in Et_2O to yield black-metallic purple crystals of **1**-Fe (0.229 g, 80%). **b.** A solution of smifH (5.00 g, 25.35 mmol) in 100 mL of THF was added dropwise to a solution of lithium bis(trimethylsilyl)amide (4.242 g, 25.35 mmol) in 50 mL of THF at −78 °C under argon. The solution turned magenta and was stirred at −78 °C for 3 h prior to the addition of $FeBr_2(THF)_2$ (4.561 g, 12.67 mmol). After stirring at 23 °C for 16 h, a purple crystalline solid precipitated from the forest green solution. The volatiles were removed in vacuo, and the residue was dissolved in toluene and filtered. Toluene was removed, and the solid was triturated with Et_2O and filtered to yield black-metallic purple crystals of **1**-Fe (2.980 g, 52%). ^{1}H NMR (C_6D_6, 400 MHz): δ 5.73 (t, py-C^5*H*, 1 H, J = 5.9 Hz), 6.11 (d, py-C^3*H*, 1 H, J = 7.9 Hz), 6.38 (t, py-C^4*H*, 1 H, J = 7.8 Hz), 7.59 (s, *CH, 1* H), 7.66 (d, py-C^6*H*, 1 H, J = 5.2 Hz). ^{13}C{^{1}H} NMR (C_6D_6, 100 MHz): δ 112.19 (*C*H), 115.64 (py-C^{3}H), 118.34 (py-C^{5}H), 134.68 (py-C^{4}H), 151.81 (py-C^{6}H), 165.65 (py-C^2). Anal. Calcd. $H_{20}C_{24}N_6Fe$: C, 64.30; H, 4.50; N, 18.75. Found: C, 63.76; H, 4.64; N, 17.69.

*11. (^{o}Mesmif)$_2$Fe (**2**-Fe).* To a solution of $Fe\{N(SiMe_3)_2\}_2(THF)$ (0.500 g, 1.11 mmol) in 15 mL of Et_2O was slowly added a solution of ^{o}MesmifH (0.471 g, 2.22 mmol) in Et_2O (10 mL) at 23 °C. The solution immediately changed from pale green to a brilliant blue. The reaction was degassed and warmed to 23 °C. Purple crystals began to precipitate from the deep blue solution while stirring for 20 h. The volatiles were removed, and the solid was triturated and filtered in Et_2O to yield purple crystals of **2**-Fe (0.311 g, 59%). ^{1}H NMR (C_6D_6, 400 MHz): δ 2.04 (s, py^{Me}-CH_3, 3 H), 6.44 (t, py^{Me}-C^4*H*, 1 H, *J* = 6.8 Hz), 6.51 (t, py-C^5*H*, 1 H, *J* = 6.8 Hz), 6.83 (d, py^{Me}-C^5*H*, 1 H, *J* = 6.8 Hz), 6.97 (br s, py^{Me}-C^3*H*, py-C^4*H*, 2 H), 7.59 (d, py-C^6*H*, 1 H, *J* = 6 Hz), 11.43 ($\nu_{1/2} \approx$ 29 Hz, C*H*, 1 H), 12.04 ($\nu_{1/2} \approx$ 46 Hz, C*H*, 1 H), 13.31 ($\nu_{1/2} \approx$ 52 Hz, py-C^3*H*, 1 H). ^{13}C{^{1}H} NMR (C_6D_6, 100 MHz): δ 25.93 (py^{Me}-CH_3), 100.75 (py^{Me}-C^{3}H), 103.26 (py^{Me}-C^{5}H), 107.54 (py-C^{3}H), 112.22 (py-C^{5}H), 114.11 (py^{Me}-C^{4}H), 119.50 (*C*H), 123.66 (py-C^{4}H), 132.93 (*C*H), 136.73 (py-C^{6}H), 149.10 (py^{Me}-C^{6}H), 160.93 (py^{Me}-C^2), 170.83 (py-C^2). Anal. Calcd $H_{24}C_{26}N_6Fe$: C, 65.56; H, 5.08; N, 17.64. Found: C, 65.58; H, 5.25; N, 17.17. μ_{eff} (SQUID, 5 K) = 0.5 μ_B to μ_{eff} (SQUID, 300 K) = 1.22 μ_B.

12. (^{o}Me$_2$smif)$_2$Fe (3-Fe). To a solution of $Fe\{N(SiMe_3)_2\}_2(THF)$ (0.747 g, 1.66 mmol) in 12 mL Et_2O was slowly added a solution of ^{o}Me$_2$smifH (0.750 g, 3.33 mmol) in Et_2O (10 mL) at 23 °C. The solution immediately changed from pale green to deep forest green. The reaction was degassed and warmed to 23 °C. Gold-bronze crystals began to precipitate from the deep cobalt blue solution after stirring for 30 min. The reaction mixture was stirred for an addition 15.5 h. The volatiles were removed, and the solid was triturated and filtered in Et_2O to yield gold-bronze crystals of **3**-Fe (0.712 g, 85%). ^{1}H NMR (C_6D_6, 400 MHz): δ −9.64 ($\nu_{1/2} \approx$ 110 Hz, C*H*, 1 H), 7.44 ($\nu_{1/2} \approx$ 17 Hz, CH_3, 3 H), 36.73 ($\nu_{1/2} \approx$ 20 Hz, py-C*H*, 1 H), 52.87 ($\nu_{1/2} \approx$ 15 Hz, py-C*H*, 1 H), 167.44 ($\nu_{1/2} \approx$ 53 Hz, py-C*H*, 1 H). Anal. Calcd $H_{28}C_{28}N_6Fe$: C, 66.67; H, 5.60; N, 16.66. Found: C, 66.54; H, 5.47; N, 16.19. μ_{eff} (SQUID, 300 K) = 5.47 μ_B.

*13. (smif)$_2$Co (**1**-Co).* To a solution of lithium bis(trimethylsilyl)-amide (0.425 g, 2.54 mmol) in 15 mL THF at −78 °C was added dropwise a solution of smifH (0.500 g, 2.53 mmol) in 10 mL THF under argon. The reaction solution immediately turned magenta and was stirred at −78 °C for an additional 2 h prior to the addition of $CoCl_2$ (0.165 g, 1.27 mmol). After stirring at 23 °C for 36 h, the solution had darkened to a deep purple-magenta. The volatiles were removed, and the residue was dissolved and filtered in toluene. Toluene was removed in vacuo, and the solid was triturated with Et_2O and filtered to yield metallic gold crystals of **1**-Co (0.501 g, 87%). ^{1}H NMR (C_6D_6, 400 MHz): δ 10.06 ($\nu_{1/2} \approx$ 50 Hz, C*H*, 1 H), 37.63 ($\nu_{1/2} \approx$ 70 Hz, py-C*H*, 1 H), 39.90 ($\nu_{1/2} \approx$ 80 Hz, py-C*H*, 1 H), 85.19 ($\nu_{1/2} \approx$ 140 Hz, py-C*H*, 1 H), 108.94 ($\nu_{1/2} \approx$ 480 Hz, py-C*H*, 1 H). Anal. Calcd (for (smif)$_2$Co·$(C_7H_8)_{0.5}$) $H_{24}C_{27.5}N_6Co$: C, 66.40; H,

dx.doi.org/10.1021/ic200376f | Inorg. Chem. 2011, 50, 12414–12436

4.86; N, 16.89. Found: C, 65.92, 64.99; H, 4.68, 4.47; N, 17.23, 16.92. μ_{eff} (SQUID, 10 K) = 1.75 μ_B and μ_{eff} (SQUID, 300 K) = 3.19 μ_B.

*14. [(smif)$_2$Co](OTf) (**1**$^+$-Co).* To a 10 mL round-bottom flask charged with 0.200 g (0.44 mmol) (smif)$_2$Co and 0.114 g (0.44 mmol) AgOTf was vacuum transferred 8 mL THF at −78 °C. The reaction mixture changed from deep purple to cobalt blue within 5 min and slowly warmed to 23 °C. After it was stirred at 23 °C for 12 h, a magenta solid precipitated from solution. The volatiles were removed in vacuo. Recrystallization of the magenta solid in THF at 80 °C under a blanket of argon for 16 h led to the formation of metallic red crystals of **1**$^+$-Co (0.215 g, 81%). ^{1}H NMR (THF-d_8, 400 MHz): δ 6.55 (t, py-C^5*H*, 1 H, J = 6.4 Hz), 6.85 (d, py-C^3*H*, 1 H, *J* = 8 Hz), 7.24 (s, C*H*, *1* H), 7.28 (t, py-C^4*H*, 1 H, *J* = 7.2 Hz), 7.59 (d, py-C^6*H*, 1 H, J = 6.0 Hz). ^{13}C{^{1}H} NMR (THF-d$_8$, 100 MHz): δ 117.47 (*C*H), 118.23 (py-*C*^{3}H), 119.54 (py-*C*^{5}H), 120.36 (py-*C*^{4}H), 139.24 (py-*C*^{6}H), 148.56 (py-*C*^{2}).

*15. (smif)$_2$Ni (**1**-Ni).* A solution of lithium bis(trimethylsilyl)amide (0.425 g, 2.54 mmol) in 15 mL THF under argon at −78 °C was slowly treated with a solution of smifH (0.500 g, 2.53 mmol) in THF (10 mL) . The solution instantly turned magenta and was stirred at −78 °C for 2 h prior to the addition of $NiCl_2$(dme) (0.278 g, 1.27 mmol). After stirring at 23 °C for 36 h, the volatiles were removed in vacuo from the magenta reaction mixture. The solid was dissolved and filtered in toluene. Toluene was removed, and the solid was triturated and filtered in Et_2O to yield metallic gold crystals of (smif)$_2$Ni (0.385 g, 67%). ^{1}H NMR (C_6D_6, 400 MHz): δ 9.40 ($\nu_{1/2} \approx$ 170 Hz, C*H*, 1 H), 51.75 ($\nu_{1/2} \approx$ 400 Hz, py-C*H*, 1 H), 57.01 ($\nu_{1/2} \approx$ 470 Hz, py-C*H*, 1 H), 140.85 ($\nu_{1/2} \approx$ 3300 Hz, py-C*H*, 1 H), 248.32 ($\nu_{1/2} \approx$ 6200 Hz, py-C*H*, 1 H). Anal. Calcd. (for (smif)$_2$Ni·(C_6H_6)$_{0.5}$) $H_{23}C_{27}N_6Ni$: C, 66.15; H, 4.73; N, 17.14. Found: C, 65.52; H, 4.61; N, 17.13. μ_{eff} (SQUID, 300 K) = 2.81 μ_B.

*16. (smif)$_2$Ru (**1**-Ru).* To a small bomb reactor charged with Na(smif) (0.400 g, 1.82 mmol) and (COD)$RuCl_2$ (0.256 g, 0.946 mmol) was vacuum transferred 15 mL THF at −78 °C. After warming to 23 °C, the bomb was heated in a 60 °C oil bath for 2 d as the magenta solution became dark green with dark purple solids. The reaction mixture was filtered cold in THF, and all volatiles were removed in vacuo. The resulting dark purple, metallic solid was washed with pentane, and 0.276 g (smif)$_2$Ru were isolated (61%). ^{1}H NMR (C_6D_6, 400 MHz): δ 5.64 (t, py-C^5*H*, 1 H, *J* = 6.4 Hz), 6.07 (d, py-C^3*H*, 1 H, *J* = 8.3 Hz), 6.81 (s, C*H*, *1* H), 6.31 (t, py-C^4*H*, 1 H, *J* = 7.6 Hz), 7.80 (d, py-C^6*H*, 1 H, *J* = 5.1 Hz). ^{13}C{^{1}H} NMR (C_6D_6, 125 MHz): δ 113.66 (CH), 113.73 (py-C^{3}H), 115.03 (py-C^{5}H), 134.77 (py-*C*^{4}H), 151.24 (py-C^{6}H), 167.54 (py-*C*^{2}). Anal. Calcd. $H_{24}C_{20}N_6Ru$: C, 58.41; H, 4.08; N, 17.03. Found: C, 58.48; H, 4.22; N, 13.28.

*17. [(smif)$_2$Rh][OTf] (**1**$^+$-Rh).* To a small bomb reactor charged with Na(smif) (0.072 g, 0.328 mmol), AgOTf (0.042 g, 0.163 mmol) and $Rh_2(TFA)_4$ (0.054 g, 0.082 mmol) was vacuum transferred 5 mL toluene at −78 °C. After it was warmed to 23 °C, the solution turned from magenta to purple and was placed in a 100 °C oil bath for 1 d. The bright blue reaction mixture was filtered and washed with toluene. All volatiles were removed in vacuo leaving a bright red metallic solid **1**$^+$-Rh (0.028 g, 53%). ^{1}H NMR (THF-d_8, 400 MHz): δ 6.51 (t, py-C^5*H*, 1 H, *J* = 6.4 Hz), 6.87 (d, py-C^3*H*, 1 H, *J* = 8.1 Hz), 6.85 (s, C*H*, *1* H), 7.29 (t, py-C^4*H*, 1 H, *J* = 7.5 Hz), 7.77 (d, py-C^6*H*, 1 H, *J* = 5.6 Hz). ^{13}C{^{1}H} NMR (THF-d_8, 125 MHz): δ 114.72 (*C*H), 118.20 (py-*C*^{3}H), 138.70 (py-C^{5}H), 148.20 (py-C^{4}H), 148.29 (py-C^{6}H), 165.22 (py-C^2). Anal. Calcd. $H_{20}C_{25}N_6O_3F_3SRh$: C, 46.60; H, 3.13; N, 13.04. Found: C, 44.39, 44.89; H, 4.95, 3.66; N, 8.87, 9.28.

*18. [(smif)$_2$Ir][BPh$_4$] (**1**$^+$-Ir).* To a small bomb reactor charged with Na(smif) (0.195 g, 0.889 mmol), $NaBPh_4$ (0.152 g, 0.444 mmol) and $IrCl_3(THT)_3$ (0.250 g, 0.444 mmol) was vacuum transferred 5 mL THF at −78 °C. Upon warming to 23 °C, the magenta solution quickly turned navy blue. The bomb was placed in a 70 °C oil bath for 2 d after which the solution was turquoise. The reaction mixture was filtered and washed in THF. All volatiles were removed in vacuo leaving dark purple metallic solid [(smif)$_2$Ir][BPh_4] (0.200 g, 50%). ^{1}H NMR (THF-d_8, 400 MHz): δ 6.36 (t, py-C^5*H*, 1 H, *J* = 6.7 Hz), 6.53 (d, py-C^3*H*, 1 H, *J* = 8.3 Hz), 6.30 (s, C*H*, *1* H), 7.03 (t, py-C^4*H*, 1 H, *J* = 7.7 Hz), 7.60 (d, py-C^6*H*, 1 H, *J* = 6.0 Hz). ^{13}C{^{1}H} NMR (THF-d_8, 125 MHz): δ 116.08 (*C*H), 138.08 (py-C^{3}H), 140.52 (py-C^{5}H), 149.47 (py-C^{4}H), 163.36 (py-C^{6}H), 169.14 (py-C^2). Anal. Calcd. $H_{40}C_{48}N_6BRh$: C, 63.78; H, 4.46; N, 9.30. Found: C, 62.22, 65.03; H, 4.84, 4.82; N, 8.02, 8.14.

EPR Spectroscopy. Solution and frozen glass EPR spectra were recorded on a JEOL continuous wave spectrometer, JES-FA200 equipped with an X-band Gunn oscillator bridge, a cylindrical mode cavity, and a helium cryostat. For all samples, a modulation frequency of 100 kHz and a time constant of 0.1 s were employed. Frequencies were close to 9.0 GHz and all spectra were obtained on freshly prepared solutions (1−10 mM in toluene) in quartz tubes with J. Young valves and were checked carefully for reproducibility. Background spectra were obtained on clean solvents at the same measurement conditions. Spectral simulations were performed using the programs W95EPR by Prof. Dr. Frank Neese[92] and ESRSIM by Prof. Dr. Høgni Weihe, University of Copenhagen, Denmark. The fittings were performed by the "chi by eye" approach. Collinear *g* and *A* tensors were used, and deviations from isotropic parameters in spectra of frozen glasses were only used when clearly justified.

Magnetic Susceptibility Measurements. Magnetic susceptibility measurements of crystalline powdered samples (10−30 mg) were performed on a Quantum Design MPMS-5 SQUID magnetometer at 10 kOe (1 T) between 5 and 300 K for all samples. All sample preparations and manipulations were performed under an inert atmosphere because of the air sensitivity of the samples. The samples were measured in gelatin capsules, and the diamagnetic contribution from the sample container was subtracted from the experimental data. Pascal's constants[67] were used to subtract diamagnetic contributions, yielding paramagnetic susceptibilities. The program julX written by E. Bill was used for (elements of) the simulation and analysis of magnetic susceptibiltiy data.[93]

Mössbauer Spectroscopy. ^{57}Fe Mössbauer spectra were recorded on a WissEl Mössbauer spectrometer (MRG-500) at 77 K in constant acceleration mode. ^{57}Co/Rh was used as the radiation source. WinNormos for Igor Pro software has been used for the quantitative evaluation of the spectral parameters (least-squares fitting to Lorentzian peaks). The minimum experimental line widths were 0.20 mms^{-1}. The temperature of the samples was controlled by an MBBC-HE0106 MÖSSBAUER He/N_2 cryostat within an accuracy of ±0.3 K. Isomer shifts were determined relative to α-iron at 298 K.

XAS Spectroscopy. XAS data were measured at the Stanford Synchrotron Radiation Lightsource using focused beamline 9−3, under ring conditions of 3 GeV and 60−100 mA. A Si(220) double-crystal monochromator was used for energy selection and a Rh-coated mirror (set to an energy cutoff of 9 keV) was utilized in combination with 30% detuning for rejection of higher harmonics. All samples were prepared as dilutions in BN and measured as transmission spectra. Sample were maintained at 10 K using an Oxford continuous flow. To check for reproducibility, 2−3 scans were measured for all samples. The energy was calibrated from Cr and Co foil spectra, with the first inflection set to 5989.0 and 7709.5 eV, respectively. A step size of 0.11 eV was used over the edge region. Data were averaged, and a smooth background was removed from all spectra by fitting a polynomial to the pre-edge region and subtracting this polynomial from the entire spectrum. Normalization of the data was accomplished by fitting a flattened polynomial or straight line to the postedge region and normalizing the edge jump to 1.0.

Computational Methods. B3LYP[94−98] geometry optimization utilized the Gaussian03 suite of programs; the 6-31G(d) basis set was employed. Tests with the larger 6-311+G(d) basis set did not reveal significant differences in the optimized geometries. No symmetry constraints were employed in geometry optimization. Where applicable, geometry optimizations were started from both a pseudo-D_{2d} structure (akin to crystal structure of (smif)$_2$Fe (**1**-**Fe**)) and/or a highly Jahn−Teller distorted starting geometry (e.g., (smif)$_2$Co (**1**-**Co**)). Calculation of the energy Hessian was performed to confirm species as minima on their respective potential energy surfaces at this level of theory. All plausible spin multiplicities were investigated for the different M(smif)$_2$ complexes. Modeling of open-shell species with

dx.doi.org/10.1021/ic200376f | Inorg. Chem. 2011, 50, 12414−12436

density functional theory employed unrestricted Kohn−Sham methods.

Electrochemistry. All electrochemical experiments were done in a glovebox. Solutions of ∼1 mM of the desired complex were prepared in THF containing 0.1 M TBAP. The electrochemical experiments were performed using a platinum electrode as the working electrode, a silver wire as a pseudoreference electrode[99] and a platinum foil as the counter electrode. A BAS-27 W potentiostat was used to perform the experiments, and data were digitally recorded using WinDaq Serial Acquisition software (DATAQ Instruments).

Single Crystal X-ray Diffraction Studies. Upon isolation, the crystals, except those of **1**-V, were covered in polyisobutenes and placed under a 173 K N_2 stream on the goniometer head of a Siemens P4 SMART CCD area detector (graphite-monochromated MoK_α radiation, λ = 0.71073 Å). The structures were solved by direct methods (SHELXS). All non-hydrogen atoms were refined anisotropically unless stated, and hydrogen atoms were treated as idealized contributions (Riding model).

*1. (smif)$_2$V (**1**-V).* A metallic gold needle (0.30 × 0.02 × 0.01 mm) was obtained from toluene at 23 °C. It was covered with polyisobutenes, placed in a goniometer at MacCHESS station A1, cooled to 100 K, and subjected to the beamline (λ = 0.97890 Å, Si monochromator). A 360° sweep of data was collected in 2° ψ-scans. A total of 4,195 reflections were collected with 4,195 determined to be symmetry independent (R_{int} = 0.0000), and 3,918 were greater than 2σ(I). Data reduction was conducted using HKL200 software,[100] and the structure was solved by direct methods and refined (F^2) using full matrix least-squares techniques and SHELXTL[101] software. A semiempirical absorption correction from equivalents was applied, and the refinement utilized $w^{-1} = \sigma^2(F_o^2) + (0.1134p)^2 + 1.3469p$, where $p = ((F_o^2 + 2F_c^2)/3)$.

*2. (smif)$_2$Cr (**1**-Cr).* A dark green plate (0.40 × 0.15 × 0.02 mm) was obtained from the slow evaporation of toluene at 23 °C. A total of 36,536 reflections were collected with 7,312 determined to be symmetry independent (R_{int} = 0.0760), and 5,019 were greater than 2σ(I). A semiempirical absorption correction from equivalents was applied, and the refinement utilized $w^{-1} = \sigma^2(F_o^2) + (0.0489p)^2 + 0.0000p$, where $p = ((F_o^2 + 2F_c^2)/3)$.

*3. [(smif)$_2$Cr]OTf (**1**$^+$-Cr).* A metallic red plate (0.30 × 0.10 × 0.03 mm) was obtained from a solution of tetrahydrofuran at −40 °C. A total of 23,529 reflections were collected with 5,637 determined to be symmetry independent (R_{int} = 0.0540), and 4,220 were greater than 2σ(I). A semiempirical absorption correction from equivalents was applied, and the refinement utilized $w^{-1} = \sigma^2(F_o^2) + (0.0583p)^2 + 0.0687p$, where $p = ((F_o^2 + 2F_c^2)/3)$.

*4. (smif)$_2$Mn (**1**-Mn).* A metallic gold plate (0.60 × 0.20 × 0.03 mm) was obtained from the slow evaporation of toluene at 23 °C. A total of 30,750 reflections were collected with 6,863 determined to be symmetry independent (R_{int} = 0.0622), and 4492 were greater than 2σ(I). A semiempirical absorption correction from equivalents was applied, and the refinement utilized $w^{-1} = \sigma^2(F_o^2) + (0.0447p)^2 + 0.0000p$, where $p = ((F_o^2 + 2F_c^2)/3)$.

*5. (smif)$_2$Fe (**1**-Fe).* A black-metallic purple block (0.45 × 0.30 × 0.20 mm) was obtained from the slow evaporation of benzene at 23 °C. A total of 25,212 reflections were collected with 5007 determined to be symmetry independent (R_{int} = 0.0497), and 3994 were greater than 2σ(*I*). A semiempirical absorption correction from equivalents was applied, and the refinement utilized $w^{-1} = \sigma^2(F_o^2) + (0.0422p)^2 + 0.9777p$, where $p = ((F_o^2 + 2F_c^2)/3)$.

*6. (smif)$_2$Co (**1**-Co).* A metallic gold thin plate (0.25 × 0.20 × 0.01 mm) was obtained after heating a solution of toluene at 80 °C for 8 h in a sealed tube under a blanket of argon and slowing cooling to room temperature. A total of 3,587 reflections were collected with 3,587 determined to be symmetry independent (R_{int} = 0.0000), and 3,406 were greater than 2σ(I). A semiempirical absorption correction from equivalents was applied, and the refinement utilized $w^{-1} = \sigma^2(F_o^2) + (0.1045p)^2 + 1.8144p$, where $p = ((F_o^2 + 2F_c^2)/3)$.

*7. [(smif)$_2$Co]OTf (**1**$^+$-Co).* A metallic red-orange rod (0.40 × 0.15 × 0.10 mm) was obtained after heating a solution of tetrahydrofuran at 80 °C for 16 h in a sealed tube under a blanket of argon and slowing cooling to room temperature. A total of 28 729 reflections were collected with 6,783 determined to be symmetry independent (R_{int} = 0.0622), and 4,835 were greater than 2σ(I). A semiempirical absorption correction from equivalents was applied, and the refinement utilized $w^{-1} = \sigma^2(F_o^2) + (0.0846p)^2 + 0.0000p$, where $p = ((F_o^2 + 2F_c^2)/3)$.

*8. (smif)$_2$Ni (**1**-Ni).* A metallic gold plate (0.60 × 0.20 × 0.03 mm) was obtained from the slow evaporation of benzene at 23 °C. A total of 25 347 reflections were collected with 5,631 determined to be symmetry independent (R_{int} = 0.0809), and 3,712 were greater than 2σ(I). A semiempirical absorption correction from equivalents was applied, and the refinement utilized $w^{-1} = \sigma^2(F_o^2) + (0.0331p)^2 + 0.8315p$, where $p = ((F_o^2 + 2F_c^2)/3)$.

■ ASSOCIATED CONTENT

Ⓢ Supporting Information

CIF files for **1**-M (M = V, Cr, Mn) and **1**$^+$-Cr (those for **1**-M (M = Fe, Co, Ni) and **1**$^+$-Co can be found in the Supporting Information of ref 48) and additional spectroscopic details and experimental considerations, including JulX fits of all SQUID data. This material is available free of charge via the Internet at http://pubs.acs.org.

■ AUTHOR INFORMATION

Corresponding Author

*Fax: 607 255 4173. E-mail: ptw2@cornell.edu.

Present Address

⊥Max-Planck Institut für Bioanorganische Chemie, Stiftstr. 34-36, D-45470 Mülheim an der Ruhr, Germany.

■ ACKNOWLEDGMENTS

P.T.W. thanks the NSF (CHE-0718030) and Cornell University, and TRC the DOE (DE-FG02-03ER15387) for financial support. S.D. thanks Cornell University for funding, and we thank Prof. Frank Neese for helpful discussions and for aid in fitting EPR spectra, and Dr. Kyle Lancaster for calculating K-edge spectra. We also thank Valerie A. Williams and Dr. Carsten Milsmann for aid in fitting of SQUID data, and Dr. Marat Khusniyarov for additional EPR spectra. Portions of this research were carried out at the Stanford Synchrotron Radiation Lightsource, a Directorate of SLAC National Accelerator Laboratory and an Office of Science User Facility operated for the U.S. Department of Energy Office of Science by Stanford University. The SSRL Structural Molecular Biology Program is supported by the DOE Office of Biological and Environmental Research, and by the National Institutes of Health, National Center for Research Resources, Biomedical Technology Program (P41RR001209).

■ REFERENCES

(1) Kauffman, G. B. *Alfred Werner—Founder of Coordination Chemistry*; Springer-Verlag: Berlin, 1966.

(2) Spingler, B.; Scanavy-Grigorieff, M.; Werner, A.; Berke, H.; Lippard, S. J. *Inorg. Chem.* **2001**, *40*, 1065−1066.

(3) Kaes, C.; Katz, A.; Hosseini, M. W. *Chem. Rev.* **2000**, *100*, 3553−3590.

(4) Constable, E. C. *Adv. Inorg. Chem.* **1989**, *34*, 1−63.

(5) Constable, E. C. *Adv. Inorg. Chem.* **1986**, *30*, 69−121.

(6) Wadman, S. H.; van der Geer, E. P. L.; Havenith, R. W. A.; Gebbink, R. J. M.; van Klink, G. P. M.; van Koten, G. *J. Organomet. Chem.* **2008**, *693*, 3188−3190.

(7) Ward, M. D.; McCleverty, J. A.; Jeffery, J. C. *Coord. Chem. Rev.* **2001**, *222*, 251−272.

(8) Ziessel, R. *Coord. Chem. Rev.* **2001**, *216*, 195−223.

(9) Dobson, J. C.; Taube, H. *Inorg. Chem.* **1968**, *7*, 254−261.

(10) Hughes, M. C.; Macero, D. J. *Inorg. Chem.* **1976**, *15*, 2040–2044.
(11) Hogg, R.; Wilkins, R. C. *J. Chem. Soc.* **1962**, 341–350.
(12) Harris, C. M.; Patil, H. R. H.; Sinn, E. *Inorg. Chem.* **1969**, *8*, 101–104.
(13) Braterman, P. S.; Song, J. I.; Peacock, R. D. *Inorg. Chem.* **1992**, *31*, 555–559.
(14) (a) Kremer, S.; Henke, W.; Reinen, D. *Inorg. Chem.* **1982**, *21*, 3013–3022. (b) Schmidt, J. D.; Brey, W. S.; Stoufer, R. C. *Inorg. Chem.* **1967**, *6*, 268–271.
(15) Henke, W.; Reinen, D. *Z. Anorg. Allg. Chem.* **1977**, *436*, 187–200.
(16) Behrens, H.; Brandl, H. *Z. Naturforsch., B: Chem. Sci.* **1967**, *22*, 1216.
(17) Behrens, H.; Brandl, H.; Lutz, K. *Z. Naturforsch., B: Chem. Sci.* **1967**, *22*, 99–100.
(18) (a) Trofimenko, S. *J. Am. Chem. Soc.* **1967**, *89*, 3170–3177. (b) Jesson, J. P.; Trofimenko, S.; Eaton, D. R. *J. Am. Chem. Soc.* **1967**, *89*, 3148–3158. (c) Trofimenko, S. *J. Am. Chem. Soc.* **1967**, *89*, 6288–6294.
(19) (a) Trofimenko, S. *Acc. Chem. Res.* **1971**, *4*, 17–22. (b) Trofimenko, S. *Chem. Rev.* **1972**, *72*, 497–509.
(20) Churchill, M. R.; Gold, K.; Maw, C. E. *Inorg. Chem.* **1970**, *9*, 1597–1604.
(21) Glerup, J.; Goodson, P. A.; Hodgson, D. J.; Michelsen, K.; Nielsen, K. M.; Weihe, H. *Inorg. Chem.* **1992**, *31*, 4611–4616.
(22) Nelson, S. M.; Rodgers, J. *J. Chem. Soc. A* **1968**, 272–276.
(23) Butcher, R. J.; Addison, A. W. *Inorg. Chim. Acta* **1989**, *158*, 211–215.
(24) Davies, C. J.; Solan, G. A.; Fawcett, J. *Polyhedron* **2004**, *23*, 3105–3114.
(25) Malassa, A.; Gorls, H.; Buchholz, A.; Plass, W.; Westerhausen, M. *Z. Anorg. Chem.* **2006**, *632*, 2355–2362.
(26) Velusamy, M.; Palaniandavar, M.; Thomas, K. R. J. *Polyhedron* **1998**, *17*, 2179–2186.
(27) Palaniandavar, M.; Butcher, R. J.; Addison, A. W. *Inorg. Chem.* **1996**, *35*, 467–471.
(28) Lions, F.; Martin, K. V. *J. Am. Chem. Soc.* **1957**, *79*, 2733–2738.
(29) Goodwin, H. A.; Lions, F. *J. Am. Chem. Soc.* **1959**, *81*, 6415–6422.
(30) Geldard, J. F.; Lions, F. *J. Am. Chem. Soc.* **1962**, *84*, 270–282.
(31) Figgins, P. E.; Busch, D. H. *J. Am. Chem. Soc.* **1960**, *82*, 820–824.
(32) Juhász, G.; Hayami, S.; Inoue, K.; Maeda, Y. *Chem. Lett.* **2003**, *32*, 882–883.
(33) Marcos, D.; Folgado, J.-V.; Beltrán-Porter, D. *Polyhedron* **1990**, *9*, 2699–2704.
(34) Wocadlo, S.; Massa, W.; Folgado, J.-V. *Inorg. Chim. Acta* **1993**, *207*, 199–206.
(35) Marcos, D.; Martinez-Mañe, R.; Folgado, J.-V.; Beltrán-Porter, A.; Beltrán-Porter, D.; Fuertes, A. *Inorg. Chim. Acta* **1989**, *159*, 11–18.
(36) Kajiwara, T.; Sensui, R.; Noguchi, T.; Kamiyama, A.; Ito, T. *Inorg. Chim. Acta* **2002**, *337*, 299–307.
(37) Nonoyama, M.; Yamasaki, K. *Inorg. Chim. Acta* **1971**, *5*, 124–128.
(38) Rowland, J. M.; Olmstead, M. M.; Mascharak, P. K. *Inorg. Chem.* **2002**, *41*, 2754–2760.
(39) Hazra, S.; Naskar, S.; Mishra, D.; Gorelsky, S. I.; Figgie, H. M.; Sheldrick, W. S.; Chattopadhyay, S. K. *Dalton Trans.* **2007**, 4143–4148.
(40) Hellyer, R. M.; Larsen, D. S.; Brooker, S. *Eur. J. Inorg. Chem.* **2009**, 1162–1171.
(41) Kern, R. J. *J. Inorg. Nucl. Chem.* **1962**, *24*, 1105–1109.
(42) Bradley, D. C.; Hursthouse, M. B.; Newing, C. W.; Welch, A. J. *J. Chem. Soc., Chem. Commun.* **1972**, 567–568.
(43) Frazier, B. A.; Wolczanski, P. T.; Lobkovsky, E. B. *Inorg. Chem.* **2009**, *48*, 11576–11585.
(44) Westerhausen, M.; Kneifel, A. N. *Inorg. Chem. Commun.* **2004**, *7*, 763–766.
(45) Jacobsen, H.; Correa, A.; Poater, A.; Costabile, C.; Cavallo, L. *Coord. Chem. Rev.* **2009**, *253*, 687–703.
(46) de Fremont, P.; Marion, N.; Nolan, S. P. *Coord. Chem. Rev.* **2009**, *253*, 862–892.
(47) Schuster, O.; Yang, L. R.; Raubenheimer, H. G.; Albrecht, M. *Chem. Rev.* **2009**, *109*, 3445–3478.
(48) Frazier, B. A.; Wolczanski, P. T.; Lobkovsky, E. B.; Cundari, T. R. *J. Am. Chem. Soc.* **2009**, *131*, 3428–3429.
(49) Di(1,3-2-pyridyl)-2-azaallyl as Chelate for Metals. CCTEC D4598–02. U.S. Patent Pending No. 12/704,170, Filed March 17, 2010.
(50) Incarvito, C.; Lam, M.; Rhatigan, B.; Rheingold, A. L.; Qin, C. J.; Gavrilova, A. L.; Bosnich, B. *J. Chem. Soc., Dalton Trans.* **2001**, 3478–3488.
(51) Clark, D. L.; Sattelberger, A. P. *Inorg. Synth.* **1997**, *31*, 307–315.
(52) (a) Olmstead, M. M.; Power, P. P.; Shoner, S. C. *Inorg. Chem.* **1991**, *30*, 2547–2551. (b) Andersen, R. A.; Faegri, K.; Green, J. C.; Haaland, A.; Lappert, M. F.; Leung, W. P.; Rypdal, K. *Inorg. Chem.* **1988**, *27*, 1782–1786.
(53) Ittel, S. D.; English, A. D.; Tolman, C. A.; Jesson, J. P. *Inorg. Chim. Acta* **1979**, *33*, 101–106.
(54) Ward, L. G. L. *Inorg. Synth.* **1971**, *13*, 154–165.
(55) Kaesz, H. D.; Albers, M. O.; Singleton, E.; Yates, J. E.; Mccormick, F. B. *Inorg. Synth.* **1989**, *26*, 249–258.
(56) Johnson, S. A.; Hunt, H. R.; Neumann, H. M. *Inorg. Chem.* **1963**, *2*, 960–962.
(57) Frazier, B. A., Ph.D. Thesis, Cornell University, 2010.
(58) (a) Liu, X.; Ellis, J. E.; Miller, T. D.; Ghalasi, P.; Miller, J. S. *Inorg. Synth.* **2004**, *34*, 96–103. (b) Manzer, L. E. *Inorg. Synth.* **1982**, *21*, 135–140.
(59) John, K. D.; Salazar, K. V.; Scott, B. L.; Baker, T. R.; Sattelberger, A. P. *Organometallics* **2001**, *20*, 296–304.
(60) Roth, J. P.; Yoder, J. C.; Won, T.-J.; Mayer, J. M. *Science* **2001**, *294*, 2524–2526.
(61) (a) Poli, R.; Cacelli, I. *Eur. J. Inorg. Chem.* **2005**, *12*, 2324–2331. (b) Petit, A.; Cacelli, I.; Poli, R. *Chem.—Eur. J.* **2006**, *12*, 813–823.
(62) Zhang, G.; Musgrave, C. B. *J. Phys. Chem. A* **2007**, *111*, 1554–1561.
(63) Hachmann, J.; Frazier, B. A.; Wolczanski, P. T.; Chan, G. K.-L. *Chem. Phys. Chem.* **2011**. DOI: 10.1002/cphc.201100286.
(64) (a) Parish, R. V. *NMR, NQR, EPR, and Mössbauer Spectroscopy in Inorganic Chemistry*; Ellis Horwood: West Sussex, England, 1990. (b) Stevens, J. G. *Hyperfine Interact.* **1983**, *148*, 71–84.
(65) Bertini, I.; Luchinat, C.; Parigi, G. Solution NMR of Paramagnetic Molecules. In *Current Methods in Inorganic Chemistry*; Elsevier: London, 2001.
(66) Figgis, B. N.; Hitchman, M. A. *Ligand Field Theory and Its Applications*; Wiley-VCH: New York, 2000.
(67) Carlin, R. L. *Magnetochemistry*; Springer-Verlag: New York, 1986.
(68) (a) Mack, J.; Stillman, M. J.; Kobayashi, N. *Coord. Chem. Rev.* **2007**, *251*, 429–453. (b) Mack, J.; Stillman, M. J. *Coord. Chem. Rev.* **2001**, *219–221*, 993–1032.
(69) (a) Güdel, H. U.; Zilian, A. *Coord. Chem. Rev.* **1991**, *111*, 33–38. (b) Colombo, M. G.; Brunold, T. C.; Riedener, T.; Güdel, H. U.; Förtsch, M.; Bürgi, H.-B. *Inorg. Chem.* **1994**, *33*, 545–550.
(70) Ichino, T.; Villano, S. M.; Gianola, A. J.; Goebbert, D. J.; Velarde, L.; Sanov, A.; Blanksby, S. J.; Zhou, X.; Hrovat, D. A.; Borden, W. T.; Lineberger, W. C. *Angew. Chem., Int. Ed.* **2009**, *48*, 8509–8511.
(71) (a) Evans, D. F. *J. Chem. Soc.* **1959**, 2003–2005. (b) Schubert, E. M. *J. Chem. Educ.* **1992**, *69*, 62.
(72) Ray, K.; Petrenko, T.; Wieghardt, K.; Neese, F. *Dalton Trans.* **2007**, 1552–1556.
(73) Ray, K.; DeBeer George, S.; Solomon, E. I.; Wieghardt, K.; Neese, F. *Chem.—Eur. J.* **2007**, *13*, 2783–2797.
(74) Ray, K.; Weyhermüller.; Neese, F.; Wieghardt, K. *Inorg. Chem.* **2007**, *44*, 5345–5360.
(75) Petrenko, T.; Ray, K.; Wieghardt, K. E.; Neese, F. *J. Am. Chem. Soc.* **2006**, *128*, 4422–4436.

(76) Herebian, D.; Wieghardt, K. E.; Neese, F. *J. Am. Chem. Soc.* **2003**, *125*, 10997−11005.
(77) (a) Spikes, G. H.; Bill, E.; Weyhermüller, T.; Wieghardt, K. *Angew. Chem., Int. Ed.* **2008**, *47*, 2973−2977. (b) Lu, C. C.; Bill, E.; Weyhermüller, T.; Bothe, E.; Wieghardt, K. *J. Am. Chem. Soc.* **2008**, *130*, 3181−3197.
(78) (a) Bart, S. C.; Chlopek, K.; Bill, E.; Bouwkamp, M. W.; Lobkovsky, E.; Neese, F.; Wieghardt, K.; Chirik, P. J. *J. Am. Chem. Soc.* **2006**, *128*, 13901−13912. (b) Sylvester, K. T.; Chirik, P. J. *J. Am. Chem. Soc.* **2009**, *131*, 8772−8773. (c) Tondreau, A. M.; Milsmann, C.; Patrick, A. D.; Hoyt, H. M.; Lobkovsky, E.; Wieghardt, K.; Chirik, P. J. *J. Am. Chem. Soc.* **2010**, *132*, 15046−15059. (d) Bowman, A. C.; Milsmann, C.; Bill, E.; Lobkovsky, E.; Weyhermüller, T.; Wieghardt, K.; Chirik, P. J. *Inorg. Chem.* **2010**, *49*, 6110−6123.
(79) (a) Nguyen, A. I.; Zarkesh, R. A.; Lacy, D. C.; Thorson, M. K.; Heyduk, A. F. *Chem. Sci.* **2011**, *2*, 166−169. (b) Nguyen, A. I.; Blackmore, K. J.; Carter, S. M.; Zarkesh, R. A.; Heyduk, A. F. *J. Am. Chem. Soc.* **2009**, *131*, 3307−3316. (c) Blackmore, K. J.; Lal, N.; Ziller, J. W.; Heyduk, A. G. *Eur. J. Inorg. Chem.* **2009**, 735−743.
(80) Stanciu, C.; Jones, M. E.; Fanwick, P. E.; Abu-Omar, M. M. *J. Am. Chem. Soc.* **2007**, *129*, 12400−12401.
(81) (a) Pierpont, C. G. *Coord. Chem. Rev.* **2001**, *219*, 415−433. (b) Pierpont, C. G. *Coord. Chem. Rev.* **2001**, *216*, 99−125.
(82) Sarangi, R.; DeBeer George, S.; Jackson Rudd, D.; Szilagyi, R. K.; Ribas, X.; Rovira, C.; Holm, R. H.; Hedman, B.; Hodgson, K. O.; Solomon, E. I. *J. Am. Chem. Soc.* **2007**, *129*, 2316−2326.
(83) Kapre, R.; Bothe, E.; Weyhermüller, T.; DeBeer George, S.; Muresan, N.; Wieghardt, K. *Inorg. Chem.* **2007**, *46*, 7827−7839.
(84) Banerjee, P.; Sproules, S.; Weyhermüller, T.; DeBeer George, S.; Wieghardt, K. *Inorg. Chem.* **2009**, *48*, 5829−5847.
(85) Krivokapic, I.; Zerara, M.; Daku, M. L.; Vargas, A.; Enachescu, C.; Ambrus, C.; Treganna-Piggott, P.; Amstutz, N.; Krausz, E.; Hauser, A. *Coord. Chem. Rev.* **2007**, *251*, 364−378.
(86) Volpe, E. C.; Wolczanski, P. T.; Lobkovsky, E. B. *Organometallics* **2010**, *29*, 364−377.
(87) Goodwin, K. V.; Pennington, W. T.; Petersen, J. D. *Inorg. Chem.* **1989**, *28*, 2016−2018.
(88) Brunschwig, B.; Sutin, N. *J. Am. Chem. Soc.* **1978**, *100*, 7568−7577.
(89) King, E. R.; Betley, T. A. *J. Am. Chem. Soc.* **2009**, *131*, 14374−14380.
(90) Sazama, G. T.; Betley, T. A. *Inorg. Chem.* **2010**, *49*, 2512−2524.
(91) Turro, N. J. *Modern Molecular Photochemistry*; University Science Books: Sausalito, CA, 1991.
(92) Neese, F.; Zumft, W. G.; Antholine, W. E.; Kroneck, P. M. H. *J. Am. Chem. Soc.* **1996**, *118*, 8692−8699.
(93) http://ewww.mpi-muelheim.mpg.de/bac/logins/bill/julX_en.php
(94) Becke, A. D. *J. Chem. Phys.* **1993**, *98*, 5648−5652.
(95) Lee, C.; Yang, W.; Parr, R. G. *Phys. Rev. B* **1988**, *37*, 785−789.
(96) Frisch, M. J.; Trucks, G. W.; Schlegel, H. B.; Scuseria, G. E.; Robb, M. A.; Cheeseman, J. R.; Montgomery, J. A.,Jr.; Vreven, T.; Kudin, K. N.; Burant, J. C.; Millam, J. M.; Iyengar, S. S.; Tomasi, J.; Barone, V.; Mennucci, B.; Cossi, M.; Scalmani, G.; Rega, N.; Petersson, G. A.; Nakatsuji, H.; Hada, M.; Ehara, M.; Toyota, K.; Fukuda, R.; Hasegawa, J.; Ishida, M.; Nakajima, T.; Honda, Y.; Kitao, O.; Nakai, H.; Klene, M.; Li, X.; Knox, J. E.; Hratchian, H. P.; Cross, J. B.; Adamo, C.; Jaramillo, J.; Gomperts, R.; Stratmann, R. E.; Yazyev, O.; Austin, A. J.; Cammi, R.; Pomelli, C.; Ochterski, J. W.; Ayala, P. Y.; Morokuma, K.; Voth, G. A.; Salvador, P.; Dannenberg, J. J.; Zakrzewski, V. G.; Dapprich, S.; Daniels, A. D.; Strain, M. C.; Farkas, O.; Malick, D. K.; Rabuck, A. D.; Raghavachari, K.; Foresman, J. B.; Ortiz, J. V.; Cui, Q.; Baboul, A. G.; Clifford, S.; Cioslowski, J.; Stefanov, B. B.; Liu, G.; Liashenko, A.; Piskorz, P.; Komaromi, I.; Martin, R. L.; Fox, D. J.; Keith, T.; Al-Laham, M. A.; Peng, C. Y.; Nanayakkara, A.; Challacombe, M.; Gill, P. M. W.; Johnson, B.; Chen, W.; Wong, M. W.; Gonzalez, C.; Pople, J. A. *Gaussian'03*, revision C.02; Gaussian, Inc.: Carnegie, PA.
(97) Nakano, H. *J. Chem. Phys.* **1993**, *99*, 7983−7992.
(98) Schmidt, M. W.; Baldridge, K. K.; Boatz, J. A.; Elbert, S. T.; Gordon, M. S.; Jensen, J. J.; Koseki, S.; Matsunaga, N.; Nguyen, K. A.; Su, S.; Windus, T. L.; Dupuis, M.; Montgomery, J. A. *J. Comput. Chem.* **1993**, *14*, 1347−1363.
(99) Mills, J. L.; Nelson, R.; Shore, S. G.; Anderson, L. B. *Anal. Chem.* **1971**, *43*, 157−159.
(100) Otwinowski, Z.; Minor, W. Macromolecular Crystallography, Part A. *Methods in Enzymology*, Vol. *276*; Carter, C. W., Sweet, Fr. R. M., Eds.; Academic Press: New York; pp 307−326.
(101) Scheldrick, G. M. *SHELXTL*, version 5.10; Bruker AXS, Inc.: Madison, WI, 1999.

NOTE ADDED AFTER ASAP PUBLICATION

Due to a production error, this paper was published on the Web on November 17, 2011, before the text corrections were implemented. The corrected version was reposted on November 18, 2011.